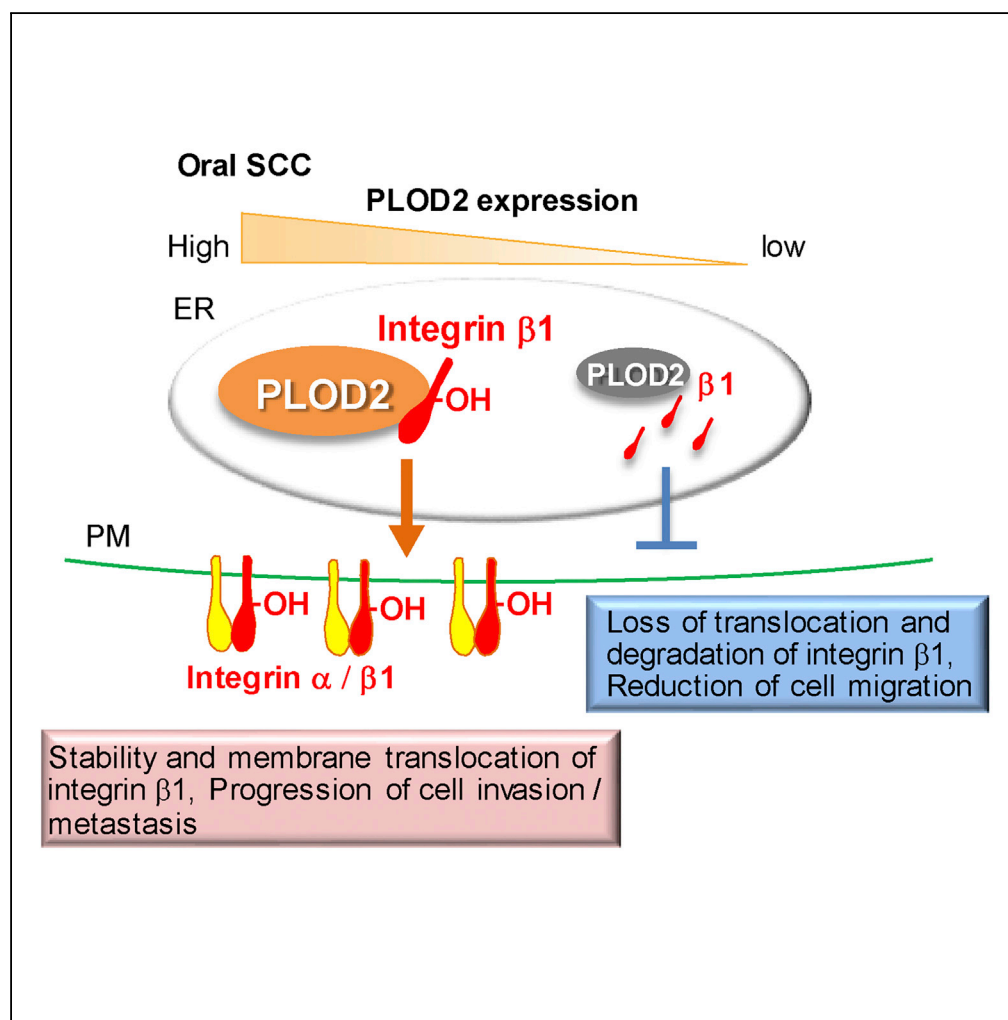


## Article

# PLOD2 Is Essential to Functional Activation of Integrin $\beta 1$ for Invasion/Metastasis in Head and Neck Squamous Cell Carcinomas



Yushi Ueki, Ken Saito, Hidekazu Iioka, ..., Masakiyo Sakaguchi, Arata Horii, Eisaku Kondo

kens@med.niigata-u.ac.jp (K.S.)  
ekondo@med.niigata-u.ac.jp (E.K.)

**HIGHLIGHTS**

PLOD2 specifically regulates intracellular localization of integrin  $\beta 1$

The hydroxylation on integrin  $\beta 1$  by PLOD2 is critical for its stability

PLOD2 and integrin  $\beta 1$  expression colocalized at the invasive front of SCC tissues

PLOD2 is necessary for tumor invasion/metastasis through the integrin  $\beta 1$  maturation

Ueki et al., iScience 23, 100850  
February 21, 2020 © 2020 The Author(s).  
<https://doi.org/10.1016/j.isci.2020.100850>

## Article

# PLOD2 Is Essential to Functional Activation of Integrin $\beta$ 1 for Invasion/Metastasis in Head and Neck Squamous Cell Carcinomas

Yushi Ueki,<sup>1,2</sup> Ken Saito,<sup>1,\*</sup> Hidekazu Iioka,<sup>1</sup> Izumi Sakamoto,<sup>3</sup> Yasuhiro Kanda,<sup>4</sup> Masakiyo Sakaguchi,<sup>5</sup> Arata Horii,<sup>2</sup> and Eisaku Kondo<sup>1,6,\*</sup>

## SUMMARY

Identifying the specific functional regulator of integrin family molecules in cancer cells is critical because they are directly involved in tumor invasion and metastasis. Here we report high expression of PLOD2 in oropharyngeal squamous cell carcinomas (SCCs) and its critical role as a stabilizer of integrin  $\beta$ 1, enabling integrin  $\beta$ 1 to initiate tumor invasion/metastasis. Integrin  $\beta$ 1 stabilized by PLOD2-mediated hydroxylation was recruited to the plasma membrane, its functional site, and accelerated tumor cell motility, leading to tumor metastasis *in vivo*, whereas loss of PLOD2 expression abrogated it. In accordance with molecular analysis, examination of oropharyngeal SCC tissues from patients corroborated PLOD2 expression associated with integrin  $\beta$ 1 at the invasive front of tumor nests. PLOD2 is thus implicated as the key regulator of integrin  $\beta$ 1 that prominently regulates tumor invasion and metastasis, and it provides important clues engendering novel therapeutics for these intractable cancers.

## INTRODUCTION

Head and neck cancers are the sixth most common malignant tumors worldwide. They are mainly treated with extended resection or radiation/chemotherapy, but functional deteriorations in swallowing, vocalization, and respiration lead to clinical decline in quality of life (QOL). Even in cases of combined surgical treatment with radiation therapy and chemotherapy, local recurrence including primary lesion and surrounding lymph nodes, is usually observed in approximately 30% of the patients. As distant metastases, as in the lung, can be seen in 25% of cases, recurrence and therapeutic resistance are very conspicuous. The 5-year survival rate in advanced cases of stage III and above is about 40%; thus the patients still present a poor prognosis (Laramore et al., 1992). Recently, cetuximab, a molecular targeting agent, has been administered in combination with cisplatin to patients with head and neck malignancies, showing some benefit to outcomes. However, it remains that subjects suffer from serious side effects such as dermatitis and mucositis, and novel avenues for cancer therapeutics are needed for improved antitumor properties and patient QOL (Bonner et al., 2006).

Previous studies revealed that 2-oxoglutarate and the iron-dependent dioxygenases superfamily function as a hydroxylase/demethylase and that they hydroxylate or demethylate molecules such as transcription factor, histones, and DNA as substrates. Indeed, it has been reported that these enzymes play various roles in cell cycle and gene expression and control of invasion/metastasis of cancer cells in multiple cell lines via modified molecules (Markolovic et al., 2015).

There are some reports that procollagen lysyl hydroxylase (PLOD), which belongs to this superfamily, is involved in the hydroxylation of collagen molecules as the only target molecule identified to date, and it is considered to be an essential enzyme for cross-linking reaction between collagen molecules outside the cell (Wu et al., 2006). PLOD is composed of an N-terminal endoplasmic reticulum-body translocation signal, a hydroxyl-catalyzed domain at the C-terminus, and hydroxylates lysine residues located in the terminal region of the collagen precursor in the ER.

Currently, three members of the PLOD family molecular group are found to share high homology: PLOD1, PLOD2, and PLOD3 (Valtavaara et al., 1997; Passoja et al., 1998a). Tissue expression analysis by Northern blot showed that PLOD2 and PLOD3 had tissue-specific expression unlike the broad expression of PLOD1.

<sup>1</sup>Division of Molecular and Cellular Pathology, Niigata University Graduate School of Medical and Dental Sciences, Asahimachi-dori, Chuo-ku, Niigata, Japan

<sup>2</sup>Department of Otolaryngology, Head and Neck Surgery, Niigata University Graduate School of Medical and Dental Sciences, Asahimachi-dori, Chuo-ku, Niigata, Japan

<sup>3</sup>ACROSCALE Inc., Kokubun-cho, Aoba-ku, Sendai, Japan

<sup>4</sup>Department of Immunology, Niigata University Graduate School of Medical and Dental Sciences, Asahimachi-dori, Chuo-ku, Niigata, Japan

<sup>5</sup>Department of Cell Biology, Okayama University Graduate School of Medicine, Dentistry and Pharmaceutical Sciences, Shikata-cho, Kita-ku, Okayama, Japan

<sup>6</sup>Lead Contact

\*Correspondence: kens@med.niigata-u.ac.jp (K.S.), ekondo@med.niigata-u.ac.jp (E.K.)

<https://doi.org/10.1016/j.isci.2020.100850>



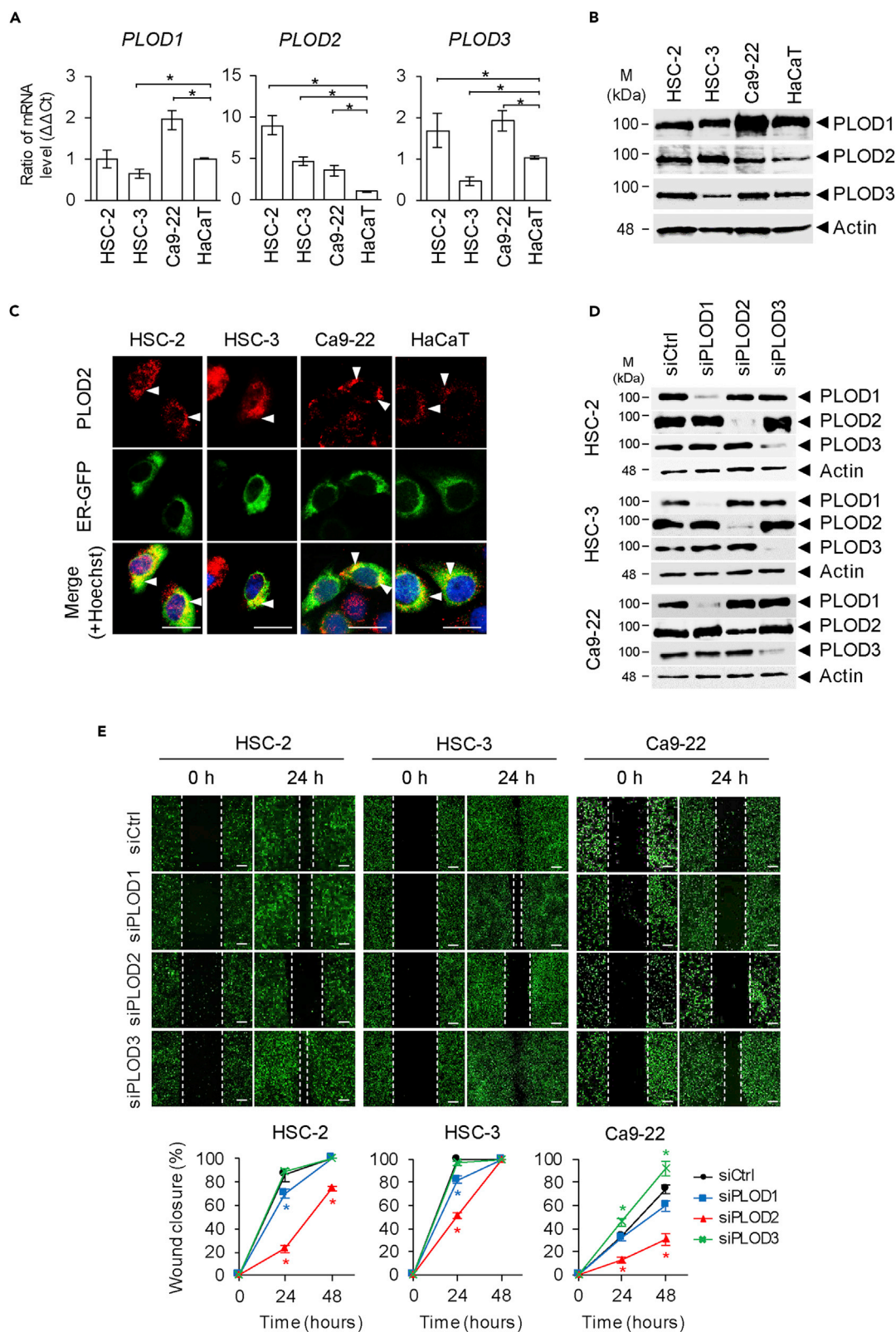


**Figure 1. Expression of the Various Hydroxylases in Oral SCC Cells**

(A) The expression level of mRNAs in oral SCC cells was determined by quantitative PCR compared with that of HaCaT. Data are means  $\pm$  s.d. from three biological replicates (\* $p < 0.05$ , Student's t-test).  
(B) Protein expression of PLOD family in SCC lines and HaCaT by immunoblotting.  
(C) Immunofluorescence of PLOD2 in oral SCC lines (HSC-2, HSC-3, and Ca9-22) and non-neoplastic keratinocyte (HaCaT). Colocalization of PLOD2 with ER marker (ER-GFP) was indicated by arrowhead. Nuclei were stained with Hoechst 33258. Scale bar = 20  $\mu$ m.  
(D) RNA interference (siRNA)-mediated knockdown of *PLOD* in oral SCCs demonstrated the attenuated protein expression by immunoblotting.  
(E) GFP-expressing SCC cells were transfected with control siRNA (siCtrl) or with *PLOD*-siRNA (siPLOD1, siPLOD2, and siPLOD3). Cell migration was evaluated by wound healing assay. Images were taken at 0 and 24 h after wound formation (scale bar = 400  $\mu$ m). The wound width was estimated using fluorescence microscopic images. Each symbol represents siCtrl (circle, black), siPLOD1 (square, blue), siPLOD2 (triangle, red), and siPLOD3 (cross, green). Asterisk indicates  $p < 0.05$  as compared with siCtrl. Data are means  $\pm$  s.d. from three technical replicates for one biological replicate.

In particular, PLOD2 has been reported to be induced in response to differentiation of bone marrow stromal cells (Valtavaara et al., 1998; Uzawa et al., 1999). Gene mutations in PLOD1 and PLOD3 have been identified in the case of Ehlers-Danlos syndrome (fragile skin, hematomas, and joint hypermobility), whereas PLOD2 mutations are clinically reported as involved in the Bruck syndrome characterized by imperfect bone formation (Walker et al., 2004; van der Slot et al., 2003).

Furthermore, based on the previous studies, PLOD2 has been reported to be specifically induced by activation of transcription factor HIF-1 $\alpha$  in response to hypoxia and TGF- $\beta$ 1 stimulation on tumor stroma, cancer cells (breast cancer, hepatocellular carcinoma), and sarcoma (mouse sarcoma model) (Chen et al., 2015; Gilkes et al., 2013a, 2013b; Eisinger-Mathason et al., 2013).

It is known that collagen secretion and remodeling of extracellular matrix (ECM) are accelerated especially in cancer stromal cells, leading to invasion and metastases of cancer cells (Gilkes et al., 2013a). The association of HIF-1 $\alpha$ -dependent increase in expression of PLOD2 and epithelial mesenchymal transition (EMT) has been established in human glioma cells, and glioma patients with high expression of PLOD2 showed a poor prognosis (Xu et al., 2017). However, the intracellular substrate and tumorigenic activity of PLOD2 expressed in cancer cells remains unclear, especially in refractory cancers, such as oral, head, and neck cancers.

In this study, apart from tumor microenvironmental factors, we focused on biological function of PLOD2 on cancer cell itself using oral squamous cell carcinoma (SCC) lines as a model because they are high in PLOD2 expression, especially in tumor invasion/metastasis highlighting specific interaction between PLOD2 and integrin  $\beta$ 1. We have found that PLOD2 induces the hydroxylation of integrin  $\beta$ 1, which plays an essential role in the stability and cellular localization of integrin  $\beta$ 1 for its functional activation. The integrin  $\beta$ 1 requires specific interaction with PLOD2, which will lead to greater understanding of molecular mechanisms for cancer invasion/metastasis and foster innovation in therapies against refractory malignancies.

**RESULTS****Specific Upregulation of PLOD2 and Its Effect on Cellular Motility of Oral SCC Cells**

Since the 2-oxoglutarate and iron-dependent dioxygenases have been classified into several groups according to the target amino acid residue, such as proline hydroxylase, asparagine/aspartate hydroxylase, etc., we first examined their expression in each category to identify specific hydroxylases highly expressed only in SCC lines from the oral cavity, in contrast to the non-neoplastic cellular counterpart (non-tumorigenic immortalized keratinocyte), HaCaT. Three representative human oral SCC lines (HSC-2, HSC-3, Ca9-22) derived from different patients were examined in comparison with HaCaT, and gene expression of typical hydroxylases for each category was examined by a semiquantitative RT-PCR method (Figure S1A). The expression of *JMJD2A*, *JMJD6*, *EGLN2*, *MINA53*, *NO66*, *HIF1AN*, *FTO*, and *TET1* did not show a significant difference between the tumor cells and HaCaT. On the other hand, the expression of *PLOD2*, *EGLN1*, *EGLN3*, *OGFOD1*, *ASPH*, and *ALKBH3* revealed certain differences in expression among these cell lines, especially in that the mRNA level of *PLOD2* in the SCC lines showed the most prominent and consistent increase at four to eight times compared with HaCaT (Figures S1A and 1A). This upregulation of *PLOD2* mRNA in tumor cells was also corroborated by protein levels in immunoblot analysis even among the lysyl hydroxylase family including PLOD1 and PLOD3 (Figure 1B). Immunofluorescence analysis with anti-PLOD2 antibody revealed that endogenous PLOD2 was predominantly localized to the ER which was confirmed by GFP-labeled ER marker (Figure 1C). Thus, tumor-specific upregulation of the expression was observed only in PLOD2 among the examined hydroxylase and demethylase family, and the mRNA and protein levels of PLOD1 and PLOD3 were not specifically elevated in the tumor cells although they are categorized to the same family.

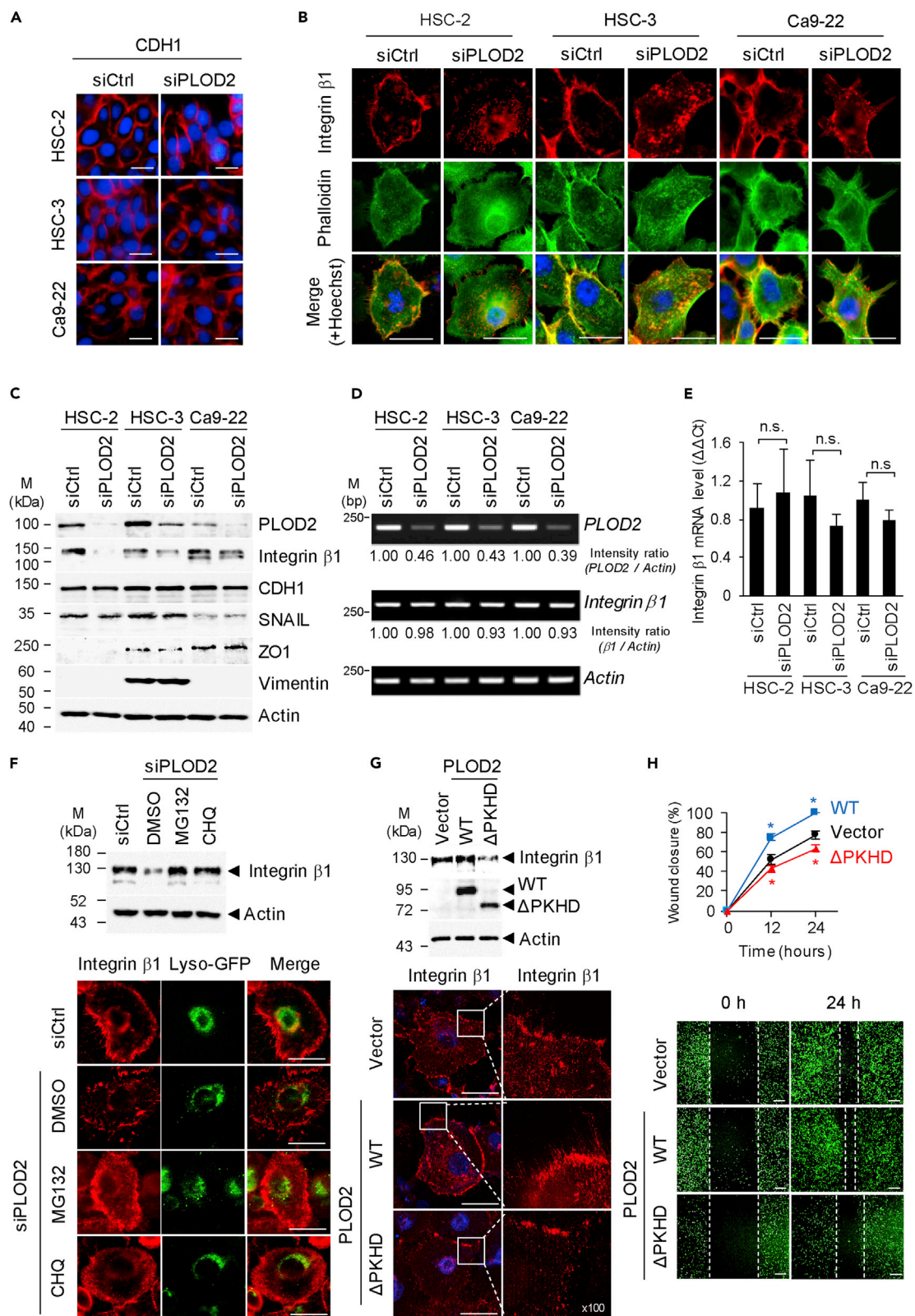


### Figure 2. PLOD2 Is Essential for Stabilization of Integrin $\beta$ 1

- (A) Immunofluorescence revealed expression, and localization of CDH1 was not affected by siPLOD2-treatment in SCC cells.
- (B) Expression and intracellular localization of integrin  $\beta$ 1 of the SCC cells was examined at 48 h after treatment with siPLOD2. Cytoskeleton and nuclei were stained with phalloidin and Hoechst, respectively. Scale bar = 20  $\mu$ m.
- (C) Expression of integrin  $\beta$ 1, CDH1, and SNAIL in the siPLOD2-transfected cells by immunoblotting using anti-PLOD2, anti-integrin  $\beta$ 1, anti-CDH1, and anti-SNAIL Ab, respectively.
- (D) Semiquantitative expression of *integrin  $\beta$ 1* mRNA by RT-PCR with or without siPLOD2-treatment.
- (E) Comparative ratio of *integrin  $\beta$ 1* mRNA in siPLOD2-treated cells based on the quantitative PCR results. Quantitative results are mean  $\pm$  s.d. from three biological replicates (n.s. = not significant, Student's t-test).
- (F) Restoration of integrin  $\beta$ 1 by treatment with MG132 and chloroquine (CHQ). HSC-2 cells pretreated with siPLOD2 were examined for integrin  $\beta$ 1 expression 18 h after treatment with MG132 (1 nM) or CHQ (50  $\mu$ M), respectively. Expression of integrin  $\beta$ 1 protein by immunoblotting (upper panel), intracellular localization of integrin  $\beta$ 1 by immunofluorescence using anti-integrin  $\beta$ 1 Ab (lower panel). Integrin  $\beta$ 1 (red) was merged with lysosome marker (Lyso-GFP). Scale bar = 20  $\mu$ m.
- (G) Effect of PLOD2 mutant lacking the catalytic domain ( $\Delta$ PKHD) to integrin  $\beta$ 1. Integrin  $\beta$ 1 of the HSC-2 transfected with myc-tagged PLOD2 lacking the hydroxylase domain ( $\Delta$ PKHD) compared with that of the cells transfected with the WT. Reduction of integrin  $\beta$ 1 detected by immunoblotting (upper panel) and the loss of plasma membrane localization indicated by arrowhead with immunofluorescence (lower panel). Scale bar = 20  $\mu$ m.
- (H) Wound healing assay revealed cell migration was affected in the  $\Delta$ PKHD-transfected cells as shown in the graph (upper panel) and migratory images (lower panel). Each symbol in the graph represents empty vector (circle, black), PLOD2 WT (square, blue), and PLOD2  $\Delta$ PKHD mutant (triangle, red). Data are means  $\pm$  s.d. from three technical replicates for one biological replicate (\* $p$  < 0.05, Student's t-test as compared with empty vector).

Based on these results, we next studied the cellular motility of the SCC cells, HSC-2, HSC-3, and Ca9-22, treated with specific siRNA against *PLOD2* (si*PLOD2*) in comparison with the cells treated with si*PLOD1* or si*PLOD3*. Specificity of the siRNA for each PLOD isoform (si*PLOD1*, si*PLOD2*, and si*PLOD3*) was confirmed by immunoblotting, which demonstrated that knockdown by these siRNAs did not affect other isoforms (Figures S1B and 1D). In the wound-healing assay, each stable GFP-expressing clone established from parental HSC-2, HSC-3, and Ca9-22 was employed for evaluation. Mobilization of each clone, visualized by fluorescence microscope 24 h after treatment with the siRNA, revealed that only attenuated expression of PLOD2 significantly affected cellular migration among these three SCC cells, whereas neither *PLOD1*-knockdown nor *PLOD3*-knockdown critically disturbed migration of the tumor cells (Figure 1E, upper images and Figure S1B). Inhibition of wound closure was over 50% in si*PLOD2*-treated cells at 24 h following siRNA treatment (Figure 1E, lower graphs); however, the MTT assay indicated that tumor cell proliferation was not affected by siRNA-treatment in all *PLOD* isoforms (Figure S1C). These data implied that PLOD2 might be deeply involved in regulating tumor cell motility.

### Crosstalk between PLOD 2 and Integrin $\beta$ 1 in Cellular Motility

On the basis of these findings, we focused on the specific role of PLOD2 in tumor cell motility. Generally, acceleration of cell mobility is closely related to invasive properties of tumor cells, and we examined whether expression of E-cadherin (CDH1) as a marker of epithelial-mesenchymal transition (EMT) was altered with or without si*PLOD2*-treatment of the SCC cells. We found that *PLOD2*-knockdown did not affect the expression and membrane localization of CDH1 for all SCC cells (Figures 2A and S2A). Because all of these three SCC lines highly express integrin  $\beta$ 1 as one of the critical motor molecules for invasion, we next examined the effect of PLOD2 on integrin  $\beta$ 1 therein. In si*PLOD2*-treated tumor cells, lack of filopodia development was observed as a morphological change as confirmed by phalloidin staining, and a marked decrease in integrin  $\beta$ 1 was revealed, in contrast to the cells treated with control siRNA (Figures 2B, S2B, S2C, and S3). This phenomenon was not seen in si*PLOD1*- or si*PLOD3*-treated cells (Figure S1D). The si*PLOD2*-treated tumor cells with decreased integrin  $\beta$ 1 showed no altered expression of CDH1 or SNAIL, suggesting the PLOD2 seemed not to be involved in EMT at least in these SCC cells (Figures 2C and S4A). Involvement of integrin  $\beta$ 1 in migration of these SCC cells was demonstrated by knockdown assay using si*Integrin  $\beta$ 1* (Figures S4B and S4C). Taken together, our data indicate that integrin  $\beta$ 1 appears directly regulated by PLOD2 for these tumor cells in an EMT-independent manner.

Next, to clarify whether PLOD2 affects induction of *integrin  $\beta$ 1* mRNA, or directly modifies the integrin  $\beta$ 1 protein, RT-PCR was first performed to examine fluctuations in mRNA levels. Ultimately, no significant alteration in *integrin  $\beta$ 1* mRNA expression with or without si*PLOD2* introduction was detected in SCC cells, which was further confirmed by qPCR (Figures 2D and 2E). Therefore, si*PLOD2* did not affect induction of *integrin  $\beta$ 1* mRNA, i.e. the result suggested that integrin  $\beta$ 1 protein might be persistently produced in tumor cells but may require a certain modification by PLOD2 for stabilization.

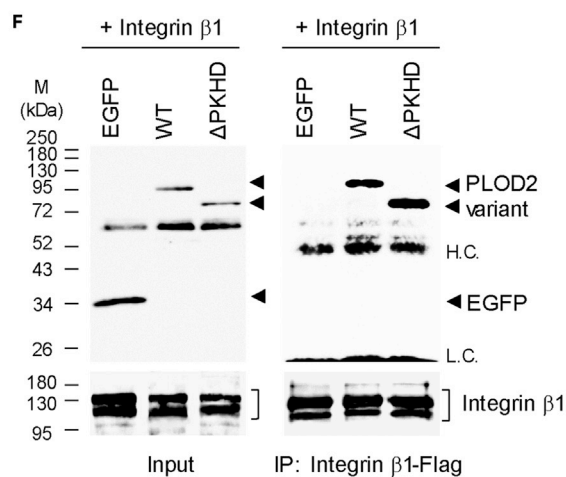
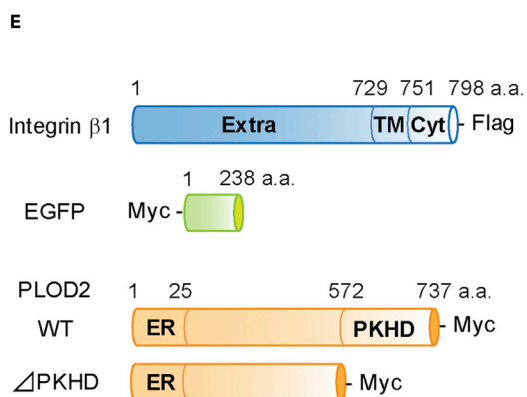
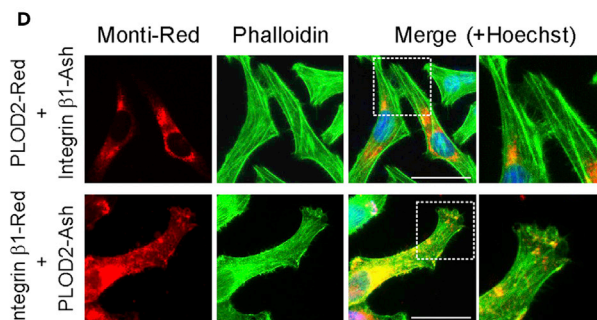
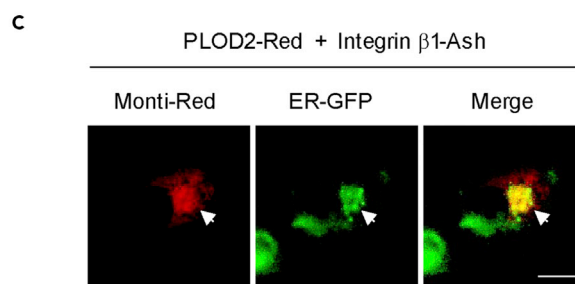
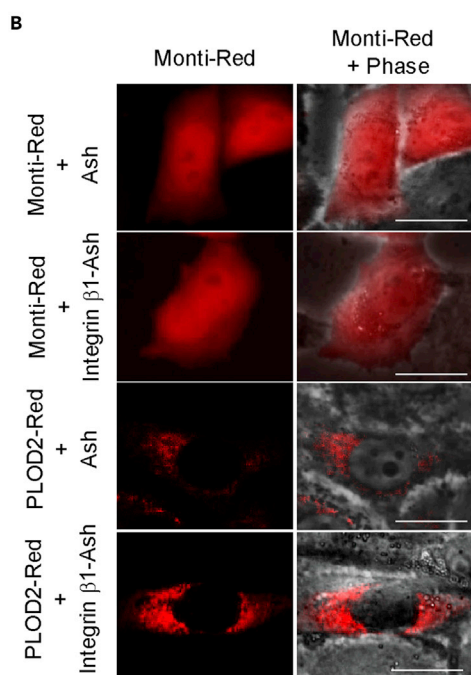
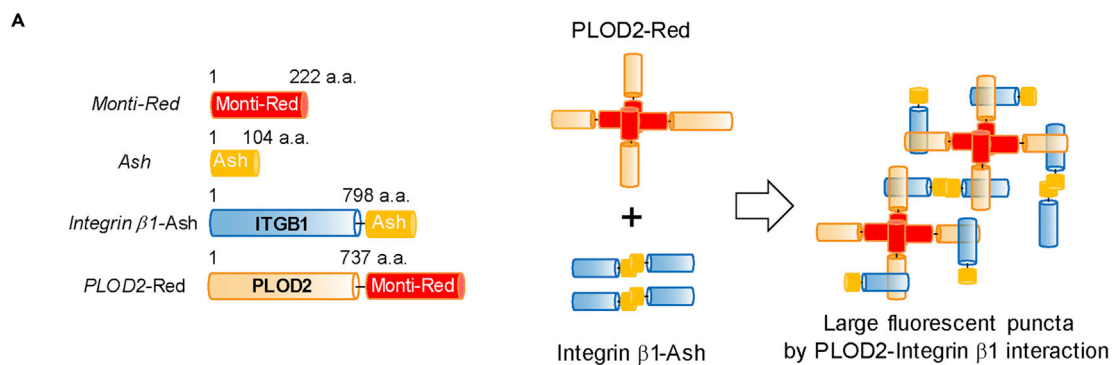


### Figure 3. Specific Coupling of Integrin $\beta 1$ with PLOD2

(A) The construction of PLOD2 expressor fused Monti-red tag (*PLOD2-Red*) and integrin  $\beta 1$  expressor fused Ash tag (*Integrin  $\beta 1$ -Ash*) (left panel). Schematic representation of mechanism for intracellular fluorescent dot formation in response to specific protein-protein interaction (right panel). (B) Marked aggregation of fluorescent dots was detected only in the HeLa cells cotransfected with *PLOD2-Red* and *Integrin  $\beta 1$ -Ash*. Scale bar = 20  $\mu\text{m}$ . (C) The fluorescent dots were merged with GFP-labeled ER marker (ER-GFP). Arrowhead indicated each PLOD2, ER-GFP, and colocalized proteins in the transfected HeLa cells, respectively. Scale bar = 20  $\mu\text{m}$ . (D) The fluorescent dots were observed at lamellipodia of the *PLOD2-Red-Integrin  $\beta 1$ -Ash* cotransfected cells or the *Integrin  $\beta 1$ -Red-PLOD2-Ash* cotransfected cells. Hatched box indicated hyperview field in the right. Scale bar = 20  $\mu\text{m}$ . (E) Domain organization of the FLAG epitope tagged-*Integrin  $\beta 1$*  expressor, Myc epitope-tagged *PLOD2* mutant expressor lacking PKHD domain ( $\Delta$ PKHD) used in the immunoprecipitation assay. (F) Integrin  $\beta 1$  was coprecipitated both with WT-PLOD2 and  $\Delta$ PKHD-PLOD2 in HEK293T cells. Expression of each PLOD2 expressor and EGFP expressor as a control in whole cell lysates (left), immunoprecipitated PLOD2, and its variant (probed with anti-Myc Ab) using anti-Flag Ab for precipitation (right). IgG heavy chain (H.C.) and light chain (L.C.) are shown.

Following the recent study reporting degradation of integrin  $\alpha$  at lysosome post-ubiquitination (Lobert et al., 2010), we examined the effects of proteasome inhibitor, MG132, and chloroquine (CHQ)—which is known to interfere with endocytosis processes and with ligand delivery to the lysosome (Erbacher et al., 1996)—as to whether they might restore the integrin  $\beta 1$  protein in si*PLOD2*-treated tumor cells. Immunoblotting demonstrated that both MG132 and CHQ successfully restore integrin  $\beta 1$  to the level of the control siRNA-treated cell as shown in Figure 2F (upper panel) and Figure S5A and that intracellular localization of integrin  $\beta 1$  was observed in the si*PLOD2*-introduced cells treated with MG132 and with CHQ, whereas membranous integrin  $\beta 1$  was only restored in MG132-treated cells (Figure S5B). The incidence of lysosome localization of integrin  $\beta 1$  remains at the same level in all cases (Figure 2F lower panel and Figure S5C). Based on this finding, the role of PLOD2 as a hydroxylase was examined with respect to stability of integrin  $\beta 1$  in the wild-type *PLOD2*-transfected HSC-2 vs. the  $\Delta$ PKHD-*PLOD2*-transfected cell ( $\Delta$ PKHD;  $\Delta$ Lysyl hydroxylase/prolyl 4-hydroxylase domain, inactive form lacking the catalytic domain of *PLOD2*) (Pirskanen et al., 1996; Passoja et al., 1998b; Heikkinen et al., 2000; Ruotsalainen et al., 2006; Kati et al., 2007). Significant enhancement of integrin  $\beta 1$  was not observed in the wild-type *PLOD2*-transfected HSC-2 but its membrane expression (filopodial localization) was prominently enhanced (Figure 2G, lower panel images) due to the stabilization of integrin  $\beta 1$  protein by sufficient PLOD2. On the other hand, immunoblotting revealed reduction of integrin  $\beta 1$  in the  $\Delta$ PKHD-*PLOD2*-transfected cells compared with empty vector or wild-type *PLOD2*-transfected HSC2 (WT), and loss of the membranous integrin  $\beta 1$  was observed in contrast to the WT and the vector cells (Figure 2G). In this regard, decrease of integrin  $\beta 1$  in  $\Delta$ PKHD-*PLOD2*-transfected cells was supposed to be due to destabilization of integrin  $\beta 1$  lacking active PLOD2, which was explained by MG132 assay shown in Figure S5D. Cellular motility of the  $\Delta$ PKHD-*PLOD2*-transfected cells was significantly attenuated as shown by wound-healing assay (Figure 2H). These data imply that hydroxylase activity of PLOD2 was required for protein stability and functional localization of integrin  $\beta 1$ .

### PLOD2 Regulates Intracellular Localization of Integrin $\beta 1$ Through Their Coupling

To examine whether PLOD2 specifically regulates intracellular localization of integrin  $\beta 1$ , "Fluorescent based technology detecting Protein-Protein Interaction in living cells" (the Fluoppi system) was employed to visualize the movement of integrin  $\beta 1$  in the presence of PLOD2 (Figure 3A). When the two proteins of interest specifically bind to each other, it yields aggregated fluorescence foci (red colored dots) inside cells under the Fluoppi system. As shown in Figure 3B, large fluorescence foci in HeLa cotransfected with *PLOD2-Red* and *integrin  $\beta 1$ -Ash* demonstrated specific binding of PLOD2 to integrin  $\beta 1$  within cells. Further we did semiquantification of fluorescent dot intensity on Fluoppi specimens between *PLOD2*-alone-expressing cells and *integrin  $\beta 1$ -PLOD2*-coexpressing cells (Figures S6A and S6B). We also repeated Fluoppi assay to obtain clear image of fluorescent dot formation only on the *integrin  $\beta 1$ -PLOD2* cotransfection into the *PLOD2*-knockout cells (Figure S6C). Tracking the *PLOD2*-integrin  $\beta 1$  complex by Fluoppi system using integrin  $\beta 1$ -Red expressor in combination with *PLOD2*-Ash, the fluorescent foci were first colocalized with ER-GFP in the early phase of transfection, suggesting they were at the ER (Figures 3C and 3D) and then Monti-red-labeled integrin  $\beta 1$  protein transited to filopodia and the plasma membrane in the cotransfected cells (Figure 3D). Immunoprecipitation assay using anti-Flag Ab on the cotransfected HEK293T cell lysates indicated binding of integrin  $\beta 1$  both to full-length *PLOD2* and  $\Delta$ PKHD-*PLOD2*, which demonstrated direct binding of these two proteins, and integrin  $\beta 1$  bound to the site outside of the PKHD domain of *PLOD2* (Figures 3E and 3F).

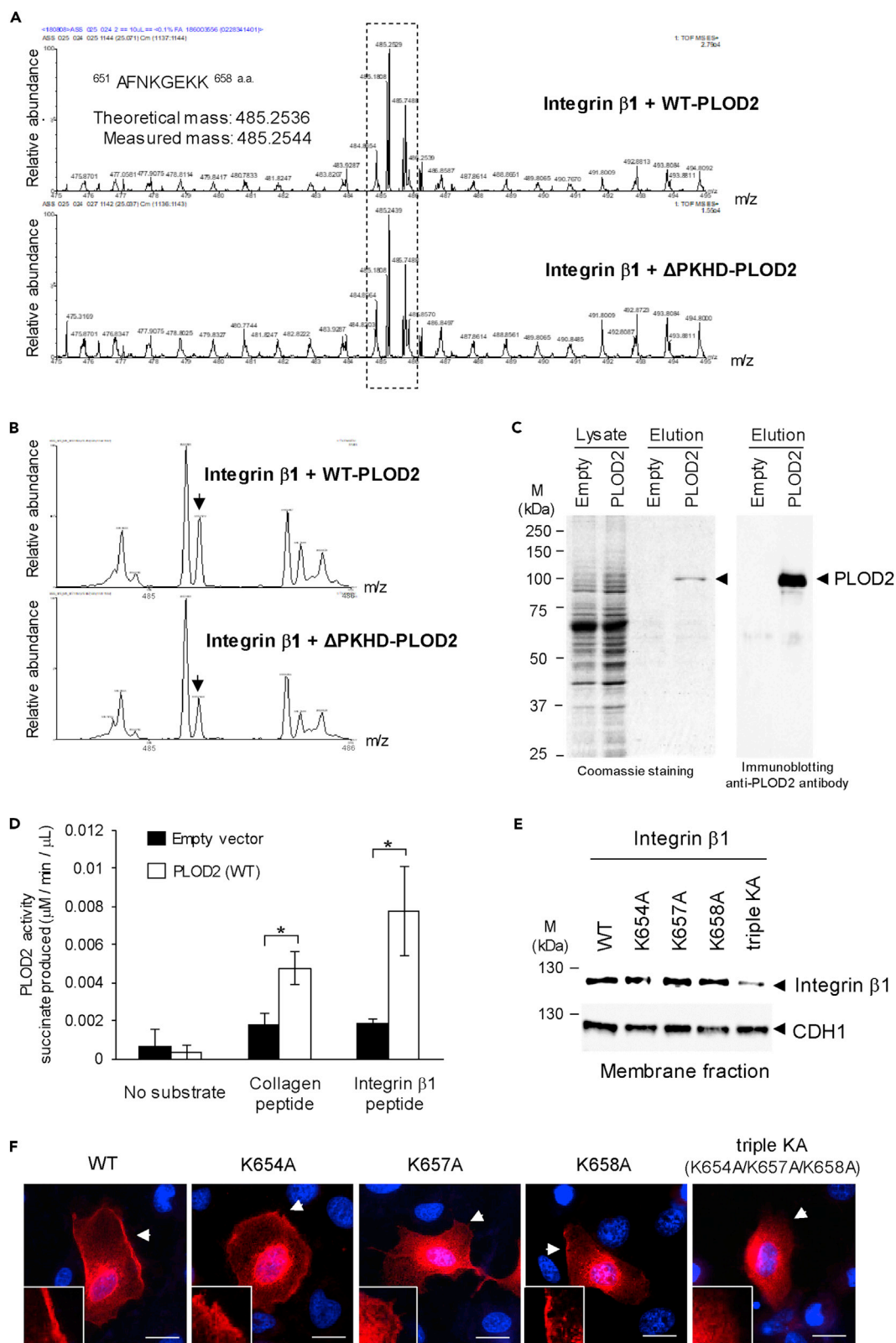


#### Figure 4. Hydroxylation of Integrin $\beta$ 1 in Presence of PLOD2 and Its Significance in Intracellular Localization of Integrin $\beta$ 1

(A) LC/MS of integrin  $\beta$ 1 purified from lysate of the 293T cells coexpressing integrin  $\beta$ 1-Flag and WT-PLOD2 in comparison with that from the cells expressing integrin  $\beta$ 1-Flag and  $\Delta$ PKHD-PLOD2. The main peaks of integrin  $\beta$ 1 were highlighted with the hatched box.

(B) Hyperview of the highlighted peaks. Arrowhead represented the fragment of integrin  $\beta$ 1 (position of #651-658 a.a. containing three lysines; AFNKGEKK) from the WT-PLOD2-transfected or from the  $\Delta$ PKHD-PLOD2-transfected lysate, which showed shift of the peak between these two integrin  $\beta$ 1 (spectra; 484.5 to 486 m/z).

(C) Recombinant PLOD2-6xHis protein from HEK293T was purified in 150 mM imidazole using cobalt resin. Purification of PLOD2 was confirmed by Coomassie staining and immunoblotting.

(D) Hydroxylation reaction of PLOD2 was carried out *in vitro* as described in [Methods](#). Collagen peptides or no peptide substrates were used as controls for reaction. Data are means  $\pm$  s.d. from three technical replicates for one biological replicate (\* $p < 0.05$ , Student's t-test).

(E) Expression of integrin  $\beta$ 1 mutants replacing Lys#654 to Ala (K654A), Lys#657 to Ala (K657A), Lys#658 to Ala (K658A), or the triple Ala-substituted mutant replacing the lysine (3KA).

(F) Intracellular localization of the integrin  $\beta$ 1 of these three mutants on HSC-2. Arrowhead indicated integrin  $\beta$ 1 at the plasma membrane. Only in the transfectant with triple Ala mutant did integrin  $\beta$ 1 lack its membranous localization. Scale bar = 20  $\mu$ m.

Further immunoprecipitation experiments of endogenous PLOD2 in HSC-2 cells revealed an interaction with the immature integrin  $\beta$ 1 ([Figure S6D](#)).

#### Direct Hydroxylation of Integrin $\beta$ 1 by PLOD2 for Its Activation

Because the result of the specific binding between PLOD2 and integrin  $\beta$ 1 would indicate that integrin  $\beta$ 1 might be a substrate for PLOD2, hydroxylation of the integrin  $\beta$ 1 protein purified from the lysate of the 293T transfected with wild-type (WT) PLOD2 was analyzed by mass spectrometry (LC/MS) using the integrin  $\beta$ 1 derived from  $\Delta$ PKHD-PLOD2 transfected cells. The main spike, indicated with the hatched box in the over-viewed LC/MS chromatogram of integrin  $\beta$ 1 from the cotransfected cells with integrin  $\beta$ 1 and WT-PLOD2 ([Figure 4A](#)), contained the unique spike (indicated by arrow) representing the molecular weight of triple lysine hydroxylation (encoded amino acids between 651 a.a. and 658 a.a., "AFNKGEKK"), which was not observed in the integrin  $\beta$ 1 protein from the integrin  $\beta$ 1- $\Delta$ PKHD-PLOD2 cotransfected sample ([Figure 4B](#); hyperview of [4A](#)). The shift of the integrin  $\beta$ 1 peak indicated by the arrow in the WT-PLOD2 cotransfected sample is two-fold higher than that of the integrin  $\beta$ 1 in the  $\Delta$ PKHD-PLOD2 cotransfected sample ([Figure 4B](#)). Additionally, we performed an experiment monitoring the activity of PLOD2 employing substrate peptides according to the previous reports ([Takaluoma et al., 2007](#); [Guo et al., 2017](#)). The result showed specific increase of succinate derived from  $\alpha$ -ketoglutarate and substrate (integrin  $\beta$ 1 substrate peptide.; AFNKGEKK) incubated with purified PLOD2 as well as positive control sample using collagen peptide (IKGIKGIK) sample ([Figures 4C and 4D](#)). The stability of integrin  $\beta$ 1 harboring the single Lys-replacement with Ala (K564A, K657A, and K658A) did not seem significantly impaired inside cells transfected with each integrin  $\beta$ 1 mutant; however, triple Lys-mutated integrin  $\beta$ 1 (K564A + K657A + K658A) seemed markedly unstable ([Figure 4E](#)). Moreover, the triple Lys-mutative integrin  $\beta$ 1 was not recruited to the plasma membrane in the transfected HSC-2 cells, in contrast to the cells with the single Lys-mutative integrin  $\beta$ 1, which still retained its membranous localization as well as in those with WT-integrin  $\beta$ 1 ([Figure 4F](#)). In this regard, flow cytometry analysis revealed that approximately 20% of the WT-transfected BHK cells showed plasma membrane expression of integrin  $\beta$ 1, whereas no significant number of cells showed membrane expression of integrin  $\beta$ 1 in the triple K-A mutant-transfected cells, which indicated loss of membrane localization without PLOD2 activity ([Figures S7A and S7B](#)). Thus, the magnitude of hydroxylation on integrin  $\beta$ 1 by PLOD2 might be critical for its intracellular stability.

#### PLOD2 Facilitates Metastasis of SCC Cells *In Vivo*

Based on these findings, we examined whether PLOD2-affected invasion/metastasis of SCC cells *in vivo* using the intrathoracic metastatic mouse model xenografted with HSC-2 cells. Stably GFP-expressing HSC-2 cells from the PLOD2-knockout clone (PLOD2-KO; KO#31, [Figure S8A](#)) were xenografted into the thoracic cavity of athymic nude (nu/nu) mice and evaluated for development of metastatic foci 40 days post-implant in comparison with mice xenografted with parental HSC-2 cells (PLOD2-WT). As to cellular behaviors, PLOD2-KO (KO#31) carrying the heterozygous knockout of PLOD2 did not show significant differences in cellular growth compared with parent HSC-2 ([Figure S8B](#)), but endogenous expression of integrin  $\beta$ 1 was seriously attenuated ([Figure S8C](#)). In the KO#31 clone, plasma membrane localization of integrin  $\beta$ 1 was also disturbed, which suggested impaired function of integrin  $\beta$ 1 ([Figure S8D](#)). Reflecting these results, cellular motility of KO#31 was also seriously decreased in comparison with the parental HSC-2 cells ([Figure S8E](#), image and graphs). Whereas, using PLOD2-KO clone (#31) of HSC-2, we performed rescue experiment by reintroducing wild-type PLOD2. The result showed the revertant (revPLOD2)

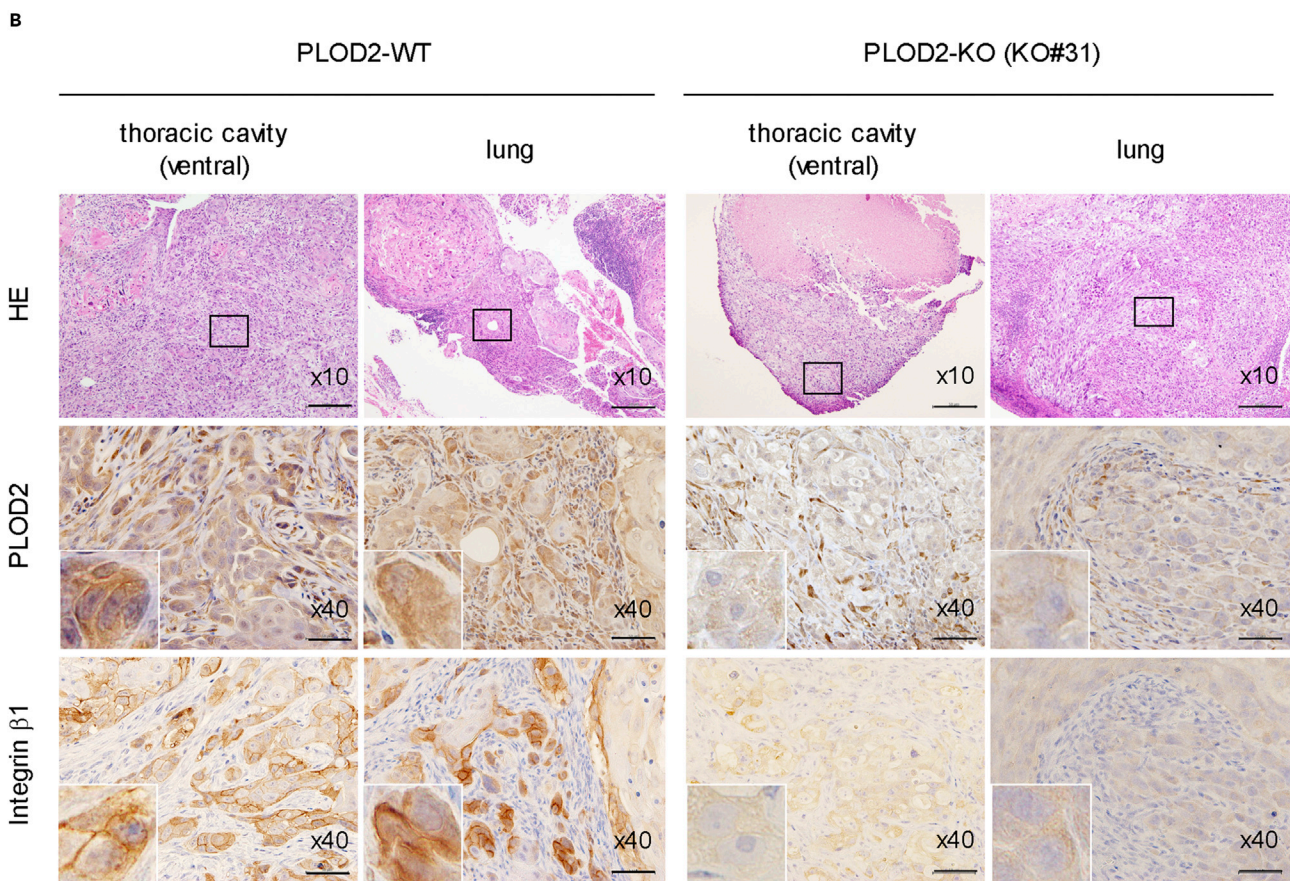
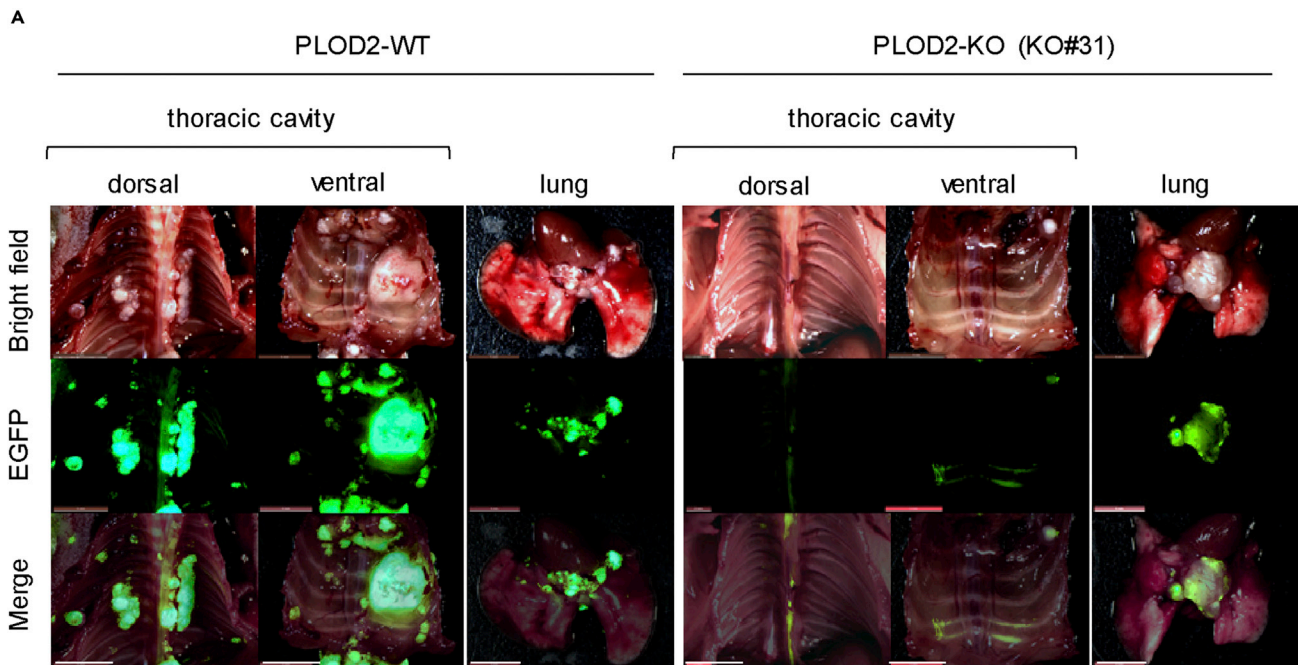


**Figure 5. Deficiency of PLOD2 Inhibited Metastasis of SCC Cells *In Vivo***

(A) *In vivo* development of metastatic foci inside thoracic cavity in mice xenografted with GFP-expressing HSC-2 bearing PLOD2-WT (left panel) and the PLOD2-deficient HSC-2 (PLOD2-KO; right panel). Fluorescence imaging was performed 40 days post-implant. (B) Histological examination of the metastatic tumor with wild type of PLOD2 (PLOD2-WT) and of that without PLOD2 (PLOD2-KO) in mice tumor models. Immunohistochemistry using anti-PLOD2 Ab and anti-integrin  $\beta$ 1 Ab were performed in the same tumor. Box at the HE images (upper panel) indicated the field shown as hyperview in the middle and lower panel. Scale bar = 50  $\mu$ m.

restored cellular motility, which was similar to the original HSC-2 by regaining expression of matured integrin  $\beta$ 1 (Figures S9A and S9B). This corroborated requirement of integrin  $\beta$ 1 expression for invasive property of HSC-2 cells, and it was regulated by PLOD2. Further we performed the time-dependent chase experiment for integrin  $\beta$ 1 under presence of PLOD2 on PLOD2-KO clone with or without WT-PLOD2 and  $\Delta$ PKHD-PLOD2 transfection. Result showed significant induction of mature integrin  $\beta$ 1 was detected in response to time-dependent increase of WT-PLOD2 (Figure S10). Whereas overexpression of  $\Delta$ PKHD-PLOD2, deficient form of hydroxylation activity (Figure 4B), induced the instability of integrin  $\beta$ 1, which suggested the necessity of hydroxylation for integrin  $\beta$ 1 maturation. Consequently, in the tumor metastasis mouse model, implant of the PLOD2-KO (KO#31) HSC-2 clone showed drastic elimination of metastatic lesions inside the thoracic cavity *in vivo* except for local growth of lung tumors, which was clearly different from the PLOD2-WT cell-implanted mice with multiple metastatic foci on pleura (Figures 5A and S11). Immunohistochemistry of the tumors derived from the PLOD2-WT cell-xenograft and KO#31 cell-xenograft was corroborative with tumor cells with or without coexpression of PLOD2 and functional integrin  $\beta$ 1 (Figure 5B).

**Coexpression of PLOD2 and Integrin  $\beta$ 1 in Oral, Pharyngeal, and Laryngeal SCC Tissues from the Patients**

Finally, endogenous expression of PLOD2 and integrin  $\beta$ 1 in SCC tissues from patients was examined. As shown in Figure 6, enhanced expression of PLOD2 was detected in SCC cells from different origins such as oral cavity (case 1, case 2: well-differentiated type; case 3: moderately differentiated type), pharynx (case 4: well-differentiated type; case 5: moderately differentiated type), and larynx (case 6: moderately differentiated type), which was consistent and coincident with integrin  $\beta$ 1 expression, especially at the marginal region and invasive front of the tumor nests (Figure S12A). Moreover, we demonstrated coexpression of these two proteins at invasive cancer nest using double immunofluorescence (Figure S12B).

**DISCUSSION**

Intracellular molecules undergoing hydroxylation by various hydroxylases have been reported to significantly alter cellular functions by regulation of protein degradation, resulting in translational activation or repression of particular proteins in various cancer cells. These intracellular events consequently affect cell-cycle progression, gene expression and activation, and the triggering of cancer invasion/metastases (Ploumakis and Coleman, 2015; Ivan et al., 2001; Zhang et al., 2009; Singleton et al., 2014). Previous studies have shown that PLOD2, one of the lysine hydroxylases, which is highly expressed in cancer cells, plays a major role to process collagens as substrate to form a suitable tumor ECM (Chen et al., 2015; Gilkes et al., 2013a, 2013b; Eisinger-Mathason et al., 2013). Accordingly, previous reports on the biological significance of PLOD2 in tumors focused on ECM regulation through its interaction with collagen fibers comprising the tumor matrix.

In this study, we found an additional functional aspect of PLOD2 as a direct regulator of cancer invasion/metastasis through its specific interaction with a major integrin family molecule, integrin  $\beta$ 1. Namely, PLOD2 is a key regulator for activation of integrin  $\beta$ 1 expressed in head and neck SCCs, which stabilizes and activates integrin  $\beta$ 1 by hydroxylation via specific binding. This event leads to accelerated cellular motility needed to form metastatic sites for the SCC cells *in vivo*. Based on results of our analysis, tumor invasion via the PLOD2-mediated activation of integrin  $\beta$ 1 seems not to be mediated by the EMT (epithelial-mesenchymal transition) process in cancer cells but by the direct effect of interactions of these two molecules. Marked increase in cellular motility of SCC cells was observed by integrin  $\beta$ 1-PLOD2 protein-protein interaction without altering CDH1 or SNAIL expression (Friedl, 2004; Friedl et al., 2004; Canel et al., 2013) as shown in Figure 2C, and the increase appeared strongly affected by catalytic activity of PLOD2 (Figures 2G, 2H, and 4D). Importantly, instability of integrin  $\beta$ 1 protein from knockdown of PLOD2 (downregulation of PLOD2) was observed in cancer cells of diverse origins such as esophageal SCC cells (KYSE30), lung adenocarcinoma cells (A549), uterine cervical SCC cells (HeLa), hepatocellular carcinoma cells (KYN-2), and breast

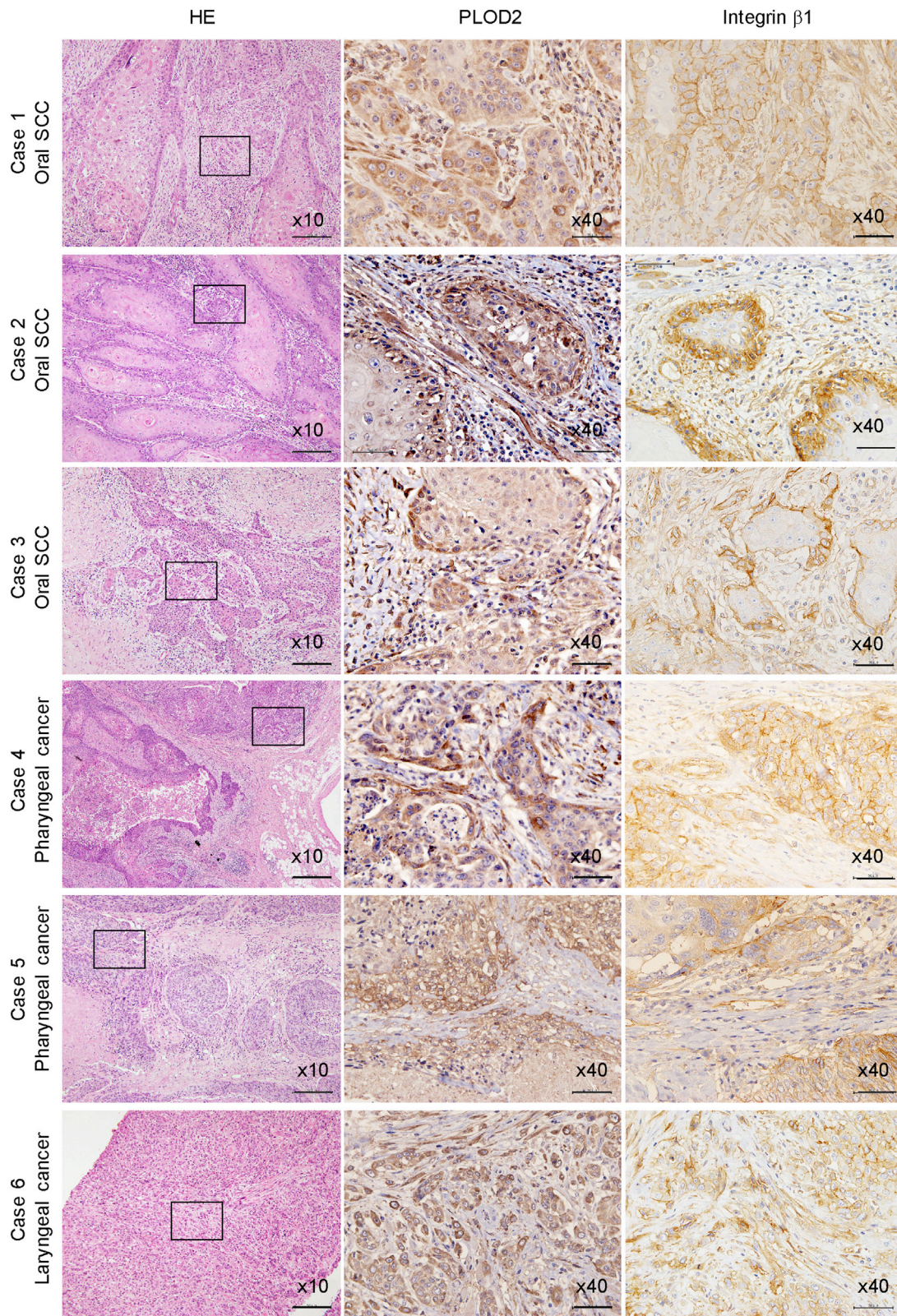


**Figure 6. Expression of PLOD2 and Integrin  $\beta$ 1 in Head and Neck SCCs from the Patients**

Immunohistochemistry using anti-PLOD2 Ab and anti-integrin  $\beta$ 1 Ab were performed on the SCC tissues derived from oral cavity, pharynx, and larynx, respectively. Box at the HE images (left column) indicated the field shown as hyperview in the middle and right column. Scale bar = 50  $\mu$ m.

invasive ductal adenocarcinoma cells (MCF7) as well (Figure S13A). In addition, we examined change of integrin  $\beta$ 6 and integrin  $\alpha$ 5 expression by treating with PLOD2-siRNA in HSC-2, HSC-3, and Ca9-22 cells, because integrin  $\beta$ 6 and  $\alpha$ 5 were reported to be expressed, in addition to  $\beta$ 1 on head/neck SCCs (Koivisto et al., 2000). The result was shown as Figure S13B, which demonstrated significant attenuation of integrin  $\beta$ 6 and  $\alpha$ 5 by PLOD2-siRNA treatment in these cells. As an exception, in HSC-3 cells, unlike other two SCC lines, decrease of  $\alpha$ 5 was not clearly observed, whereas integrin  $\beta$ 6 was decreased as well as  $\beta$ 1. This might be because of the HSC-3's different cellular property from HSC-2 and Ca9-22 (both were cloned from primary SCC lesion), which was cloned from the lymph nodal metastasis and with highly expressed Vimentin (Figure 2C). These observations imply that PLOD2 might play a pivotal role for regulation of integrin  $\beta$ 1 involved in invasion/metastasis of tumors with diverse lineages. Additionally, integrin  $\beta$ 1 knockdown had less of an effect on migration in Figure S4B, than siPLOD2 throughout. PLOD2 may in fact provide an approach to target integrin  $\beta$ 1 along with some other invasion-promoting targets. A large screening for PLOD2 targets may be required in the future.

We demonstrated that PLOD2 hydroxylase modified integrin  $\beta$ 1 protein as a direct substrate. In the intracellular molecular binding assay (Fluoppi assay), PLOD2 and integrin  $\beta$ 1 formed complex at the ER (ER) as shown in Figures 3B, 3C, and S6, then the integrin  $\beta$ 1 moved to filopodia and the plasma membrane (Figure 3D). ER localization of PLOD2 has been reported in the previous studies (Chen et al., 2017; Gjaltema et al., 2016), which is consistent with our present result, indicating that PLOD2 first hydroxylizes integrin  $\beta$ 1 at the ER, following which the integrin  $\beta$ 1 is recruited to the cell surface functional site after the modification.

In previous studies on modification of collagen by PLOD2, hydroxylation of lysine within the X-K-G motif was reported to be essential for polymerization of collagen fibers (Kivirikko and Pihlajaniemi, 1998; Myllyharju and Kivirikko, 2004; Takaluoma et al., 2007; van der Slot et al., 2003). Based on earlier findings, the putative lysine-rich motif for hydroxylation was found at position of #651-658 a.a., "AFNKGEKK," in integrin  $\beta$ 1 (Figure S13C), which may point to a target motif for PLOD2. In fact, the mass spectrometry result revealed "AFNKGEKK" as the supershifted peak among integrin  $\beta$ 1 fragments, which appeared only in the active PLOD2-treated sample (Figures 4A and 4B), and coincidentally, the triple Lys substitution with Ala (K654A/K657A/K658A) abolished membrane localization of integrin  $\beta$ 1 (Figures 4F and S7). Taking these together, the hydroxylation of these lysine within AFNKGEKK sequence by PLOD2 is critically implicated in gain of integrin  $\beta$ 1 function *in vivo*.

We generated the PLOD2-knockout HSC-2 clone, PLOD2-KO (KO#31; heterozygous genomic knockout of PLOD2, PLOD2<sup>-/+</sup>), and tracked its dynamics *in vivo* in comparison with those of the parental HSC-2 (wild type; PLOD2-WT) using the mouse xenografted model. Intrathoracic implant of PLOD2-KO cells showed loss of pleural dissemination and pulmonary metastasis; it only showed local growth of tumor, whereas PLOD2-WT cells developed multiple metastatic foci covering the entire thoracic cavity. These data suggested that cancer cell motility was critically regulated by the presence of PLOD2. Immunohistochemistry demonstrated coexpression of PLOD2 and integrin  $\beta$ 1 at invasive cancer nests in the metastatic tumor tissue derived from the mice implanted with PLOD2-WT cells, whereas integrin  $\beta$ 1 expression in cancer nests was markedly attenuated by defect in PLOD2. This histological finding corroborated the significant relationship between integrin  $\beta$ 1 and PLOD2 *in vivo* as was proven, further, by *in vitro* molecular assay. Finally, we confirmed that the expression pattern of integrin  $\beta$ 1 and PLOD2 in SCC tissues surgically obtained from patients was similar to that of tumors in the mouse model.

Therefore, we conclude that integrin  $\beta$ 1, a critical motor molecule for SCC invasion/metastasis, requires PLOD2 for its stabilization and functional cellular localization via their specific interaction through hydroxylation (Figure 7). Our results indicate that specific suppression of PLOD2 activity may provide one of the chief clues for inhibiting cancer invasion/metastasis in future cancer therapeutics.

**Limitations of the Study**

This study provides a crosstalk between PLOD 2 and integrin  $\beta$ 1 in cellular motility, and the hydroxylation on integrin  $\beta$ 1 by PLOD2 is critical for its intracellular stability. However, we could not optimize the *in vitro*

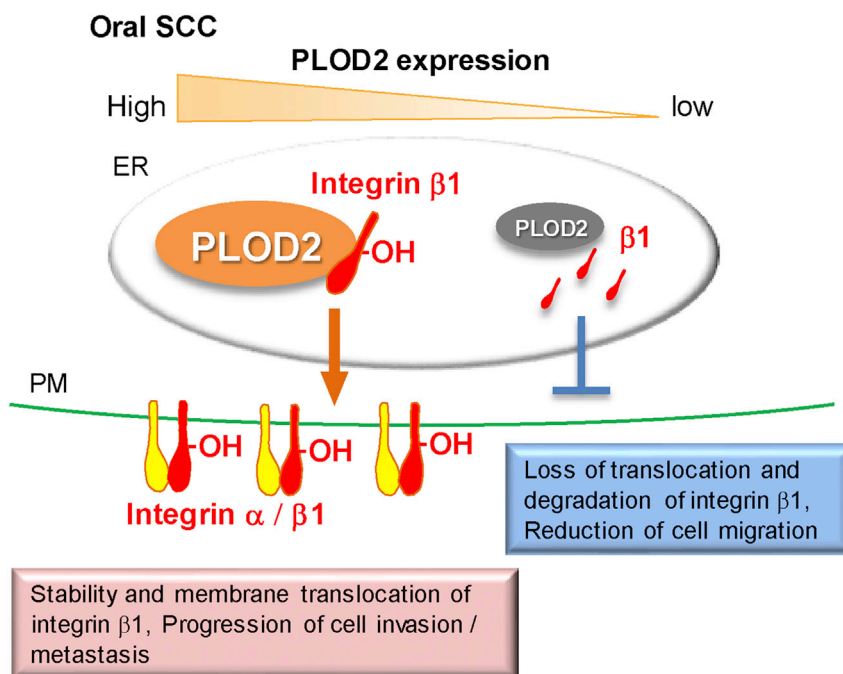


**Figure 7. Intracellular Dynamics of Integrin  $\beta 1$  Mediated by PLOD2 in SCC Cells**

Head and neck squamous cell carcinomas retain high-level expression of PLOD2, which induces hydroxylation of integrin  $\beta 1$ . Integrin  $\beta 1$  protein is stabilized by the hydroxylation and recruited to cell membrane as its functional site, which contributes to invasion/metastasis of SCCs. Loss of PLOD2 by contrast causes instability of integrin  $\beta 1$ , which results in loss of tumor metastasis. PM (plasma membrane), ER (endoplasmic reticulum), integrin  $\alpha$  (yellow), and  $\beta 1$  (red).

reaction of integrin  $\beta 1$  hydroxylation, because of an insoluble integrin  $\beta 1$  mutant substrate, and we were unable to directly detect the function of PLOD2 and integrin  $\beta 1$  in patient-derived primary SCC samples. Further enzymatically and clinically studies remain to be determined.

## METHODS

All methods can be found in the accompanying [Transparent Methods supplemental file](#).

## SUPPLEMENTAL INFORMATION

Supplemental Information can be found online at <https://doi.org/10.1016/j.isci.2020.100850>.

## ACKNOWLEDGMENTS

We thank Dr. K. Honma and Dr. T. Kawasaki (Niigata Cancer Center Hospital) for pathological informations. The collaboration was approved both by Niigata University ethical committee and Niigata Cancer Center ethical committee. We thank Dr. K. Myrick for critical reading of the manuscript. We are also grateful to Ms. A. Ageishi and Ms. N. Sumi for kind assistance for office procedures. This work was supported by Grant-in-Aid for Challenging Exploratory Research (Grant Number JP 24659170; K.S.), JAPAN SOCIETY FOR THE PROMOTION OF SCIENCE (JSPS).

## AUTHOR CONTRIBUTIONS

Conceptualization, K.S., E.K.; Methodology, Y.U., K.S.; Investigation, Y.U., K.S., H.I., I.S., Y.K., M.S.; Writing—Original Draft, K.S., E.K.; Writing—Review & Editing, E.K.; Funding Acquisition, Y.U., K.S., E.K.; Resources, Y.U., K.S., A.H.; Supervision, E.K.

## DECLARATION OF INTERESTS

The authors declare no competing interests.

Received: May 25, 2019  
 Revised: September 20, 2019  
 Accepted: January 14, 2020  
 Published: February 21, 2020

## REFERENCES

- Bonner, J.A., Harari, P.M., Giralt, J., Azarnia, N., Shin, D.M., Cohen, R.B., Jones, C.U., Sur, R., Raben, D., Jassem, J., et al. (2006). Radiotherapy plus cetuximab for squamous-cell carcinoma of the head and neck. *N. Engl. J. Med.* 354, 567–578.
- Canel, M., Serrels, A., Frame, M.C., and Brunton, V.G. (2013). E-cadherin-integrin crosstalk in cancer invasion and metastasis. *J. Cell Sci.* 126, 393–401.
- Chen, Y., Terajima, M., Yang, Y., Sun, L., Ahn, Y.H., Pankova, D., Puperi, D.S., Watanabe, T., Kim, M.P., Blackmon, S.H., et al. (2015). Lysyl hydroxylase 2 induces a collagen cross-link switch in tumor stroma. *J. Clin. Invest.* 125, 1147–1162.
- Chen, Y., Terajima, M., Banerjee, P., Guo, H., Liu, X., Yu, J., Yamauchi, M., and Kurie, J.M. (2017). FKBP65-dependent peptidyl-prolyl isomerase activity potentiates the lysyl hydroxylase 2-driven collagen cross-link switch. *Sci. Rep.* 7, 46021.
- Eisinger-Mathason, T.S., Zhang, M., Qiu, Q., Skuli, N., Nakazawa, M.S., Karakasheva, T., Mucaj, V., Shay, J.E., Stangenberg, L., Sadri, N., et al. (2013). Hypoxia-dependent modification of collagen networks promotes sarcoma metastasis. *Cancer Discov.* 3, 1190–1205.
- Erbacher, P., Roche, A.C., Monsigny, M., and Midoux, P. (1996). Putative role of chloroquine in gene transfer into a human hepatoma cell line by DNA/lactosylated polylysine complexes. *Exp. Cell Res.* 225, 186–194.
- Friedl, P. (2004). Preshaping and plasticity: shifting mechanisms of cell migration. *Curr. Opin. Cell Biol.* 16, 14–23.
- Friedl, P., Hegerfeldt, Y., and Tusch, M. (2004). Collective cell migration in morphogenesis and cancer. *Int. J. Dev. Biol.* 48, 441–449.
- Gilkes, D.M., Bajpai, S., Chaturvedi, P., Wirtz, D., and Semenza, G.L. (2013a). Hypoxia-inducible factor 1 (HIF-1) promotes extracellular matrix remodeling under hypoxic conditions by inducing P4HA1, P4HA2, and PLOD2 expression in fibroblasts. *J. Biol. Chem.* 288, 10819–10829.
- Gilkes, D.M., Bajpai, S., Wong, C.C., Chaturvedi, P., Hubbi, M.E., Wirtz, D., and Semenza, G.L. (2013b). Procollagen lysyl hydroxylase 2 is essential for hypoxia-induced breast cancer metastasis. *Mol. Cancer Res.* 11, 456–466.
- Gjaltema, R.A., van der Stoep, M.M., Boersema, M., and Bank, R.A. (2016). Disentangling mechanisms involved in collagen pyridinoline cross-linking: the immunophilin FKBP65 is critical for dimerization of lysyl hydroxylase 2. *Proc. Natl. Acad. Sci. U S A* 113, 7142–7147.
- Guo, H.F., Cho, E.J., Devkota, A.K., Chen, Y., Russell, W., Phillips, G.N., Jr., Yamauchi, M., Dalby, K.N., and Hurie, J.M. (2017). A Scalable lysyl hydroxylase 2 expression system and luciferase-based enzymatic activity assay. *Arch. Biochem. Biophys.* 618, 45–51.
- Heikkinen, J., Risteli, M., Wang, C., Latvala, J., Rossi, M., Valtavaara, M., and Myllylä, R. (2000). Lysyl hydroxylase 3 is a multifunctional protein possessing collagen glucosyltransferase activity. *J. Biol. Chem.* 275, 36158–36163.
- Ivan, M., Kondo, K., Yang, H., Kim, W., Valiando, J., Ohh, M., Salic, A., Asara, J.M., Lane, W.S., and Kaelin, W.G., Jr. (2001). HIF $\alpha$  targeted for VHL-mediated destruction by proline hydroxylation: implications for O<sub>2</sub> sensing. *Science* 292, 464–468.
- Kati, T., Juha, L., and Johanna, M. (2007). Lysyl hydroxylase 2 is a specific telopeptide hydroxylase, while all three isoenzymes hydroxylate collagenous sequences. *Matrix Biol.* 26, 396–403.
- Kivirikko, K.I., and Pihlajaniemi, T. (1998). Collagen hydroxylases and the protein disulfide isomerase subunit of prolyl 4-hydroxylases. *Adv. Enzymol. Relat. Areas Mol. Biol.* 72, 325–398.
- Koivisto, L., Grenman, R., Heino, J., and Larjava, H. (2000). Integrin  $\alpha 5 \beta 1$ ,  $\alpha v \beta 1$ , and  $\alpha v \beta 6$  collaborate in squamous cell spreading and migration on fibronectin. *Exp. Cell Res.* 255, 10–17.
- Laramore, G.E., Scott, C.B., al-Sarraf, M., Haselow, R.E., Ervin, T.J., Wheeler, R., Jacobs, J.R., Schuller, D.E., Gahbauer, R.A., Schwade, J.G., et al. (1992). Adjuvant chemotherapy for resectable squamous cell carcinomas of the head and neck: report on Intergroup Study 0034. *Int. J. Radiat. Oncol. Biol. Phys.* 23, 705–713.
- Lobert, V.H., Brech, A., Pedersen, N.M., Wesche, J., Oppelt, A., Malerød, L., and Stenmark, H. (2010). Ubiquitination of  $\alpha 5 \beta 1$  integrin controls fibroblast migration through lysosomal degradation of fibronectin-integrin complexes. *Dev. Cell* 19, 148–159.
- Markolovic, S., Wilkins, S.E., and Schofield, C.J. (2015). Protein hydroxylation catalyzed by 2-oxoglutarate-dependent oxygenases. *J. Biol. Chem.* 290, 20712–20722.
- Myllyharju, J., and Kivirikko, K.I. (2004). Collagens, modifying enzymes and their mutations in humans, flies and worms. *Trends Genet.* 20, 34–45.
- Passoja, K., Rautavuoma, K., Ala-Kokko, L., Kosonen, T., and Kivirikko, K.I. (1998a). Cloning and characterization of a third human lysyl hydroxylase isoform. *Proc. Natl. Acad. Sci. U S A* 95, 10482–10486.
- Passoja, K., Myllyharju, J., Pirskanen, A., and Kivirikko, K.I. (1998b). Identification of arginine-700 as the residue that binds the C-5 carboxyl group of 2-oxoglutarate in human lysyl hydroxylase 1. *FEBS Lett.* 434, 145–148.
- Pirskanen, A., Kaimio, A.M., Myllylä, R., and Kivirikko, K.I. (1996). Site-directed mutagenesis of human lysyl hydroxylases expressed in insect cells. Identification of histidine residues and aspartic acid residue critical for catalytic activity. *J. Biol. Chem.* 271, 9398–9402.
- Ploumakis, A., and Coleman, M.L. (2015). OH, the places you'll go! Hydroxylation, gene expression, and cancer. *Mol. Cell* 58, 729–741.
- Ruotsalainen, H., Sipilä, L., Vapola, M., Sormunen, R., Salo, A.M., Uitto, L., Mercer, D.K., Robins, S.P., Risteli, M., Attila, A., et al. (2006). Glycosylation catalyzed by lysyl hydroxylase 3 (LH3) is essential for basement membranes. *J. Cell Sci.* 119, 625–635.
- Singleton, R.S., Liu-Yi, P., Formenti, F., Ge, W., Sekimik, R., Fischer, R., Adam, J., Pollard, P.J., Wolf, A., Thalhammer, A., et al. (2014). OGFOD1 catalyzes prolyl hydroxylation of RPS23 and is involved in translation control and stress granule formation. *Proc. Natl. Acad. Sci. U S A* 111, 4031–4036.
- Takaluoma, K., Lantto, J., and Myllyharju, J. (2007). Lysyl hydroxylase 2 is a specific telopeptide hydroxylase, while all three isoenzymes hydroxylate collagenous sequences. *Matrix Biol.* 26, 396–403.
- Uzawa, K., Grzesik, W.J., Nishiura, T., Kuznetsov, S.A., Robey, P.G., Brenner, D.A., and Yamauchi, M. (1999). Differential expression of human lysyl hydroxylase genes, lysine hydroxylation, and cross-linking of type I collagen during osteoblastic differentiation in vitro. *J. Bone Miner. Res.* 14, 1272–1280.
- van der Slot, A.J., Zuurmond, A.M., Bardoel, A.F., Wijmenga, C., Puijts, H.E., Sillence, D.O., Brinckmann, J., Abraham, D.J., Black, C.M., Verzijl, N., et al. (2003). Identification of PLOD2 as telopeptide lysyl hydroxylase, an important enzyme in fibrosis. *J. Biol. Chem.* 278, 40967–40972.
- Valtavaara, M., Papponen, H., Pirttilä, A.-M., Hiltunen, K., Helander, H., and Myllylä, R. (1997). Cloning and characterization of a novel human lysyl hydroxylase isoform highly expressed in pancreas and muscle. *J. Biol. Chem.* 272, 6831–6834.
- Valtavaara, M., Szpirer, C., Szpirer, J., and Myllylä, R. (1998). Primary structure, tissue distribution, and chromosomal localization of a novel isoform

of lysyl hydroxylase (lysyl hydroxylase 3). *J. Biol. Chem.* 273, 12881–12886.

Walker, L.C., Overstreet, M.A., Willing, M.C., Marini, J.C., Cabral, W.A., Pals, G., Bristow, J., Atsawasuwan, P., Yamauchi, M., and Yeowell, H.N. (2004). Heterogeneous basis of the type VI form of Ehlers-Danlos syndrome (EDS VI) that is unrelated to decreased collagen lysyl hydroxylation. *Am. J. Med. Genet. A* 131, 155–162.

Wu, J., Reinhardt, D.P., Batmunkh, C., Lindenmaier, W., Far, R.K., Notbohm, H., Hunzelmann, N., and Brinckmann, J. (2006). Functional diversity of lysyl hydroxylase 2 in collagen synthesis of human dermal fibroblasts. *Exp. Cell Res.* 312, 3485–3494.

Xu, Y., Zhang, L., Wei, Y., Zhang, X., Xu, R., Han, M., Huang, B., Chen, A., Li, W., Zhang, Q., et al. (2017). Procollagen-lysine 2-oxoglutarate 5-

dioxygenase 2 promotes hypoxia-induced glioma migration and invasion. *Oncotarget* 8, 23401–23413.

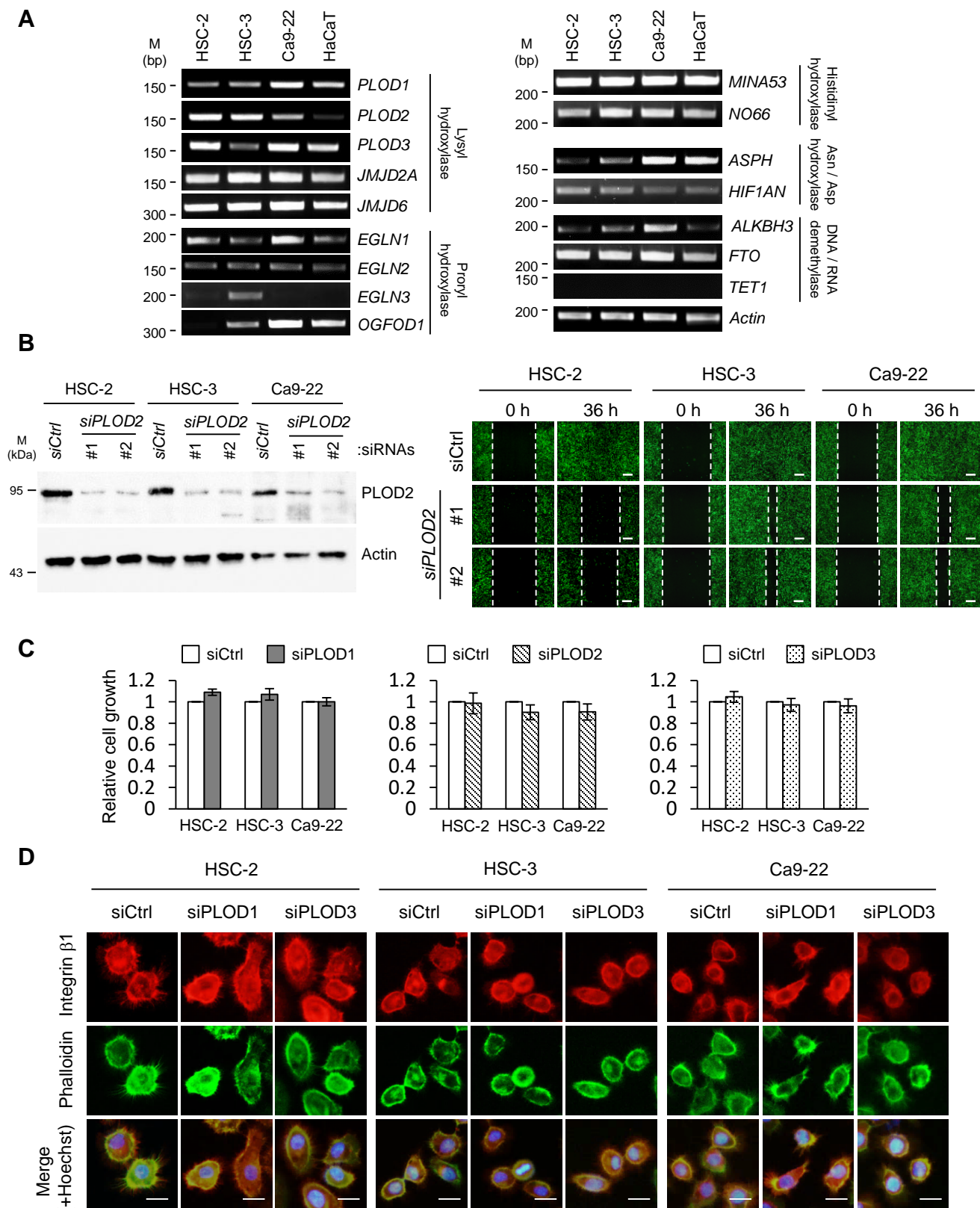
Zhang, Q., Gu, J., Li, L., Liu, J., Luo, B., Cheung, H.W., Boehm, J.S., Ni, M., Geisen, C., Root, D.E., et al. (2009). Control of cyclin D1 and breast tumorigenesis by the EglN2 prolyl hydroxylase. *Cancer Cell* 16, 413–424.

iScience, Volume 23

## **Supplemental Information**

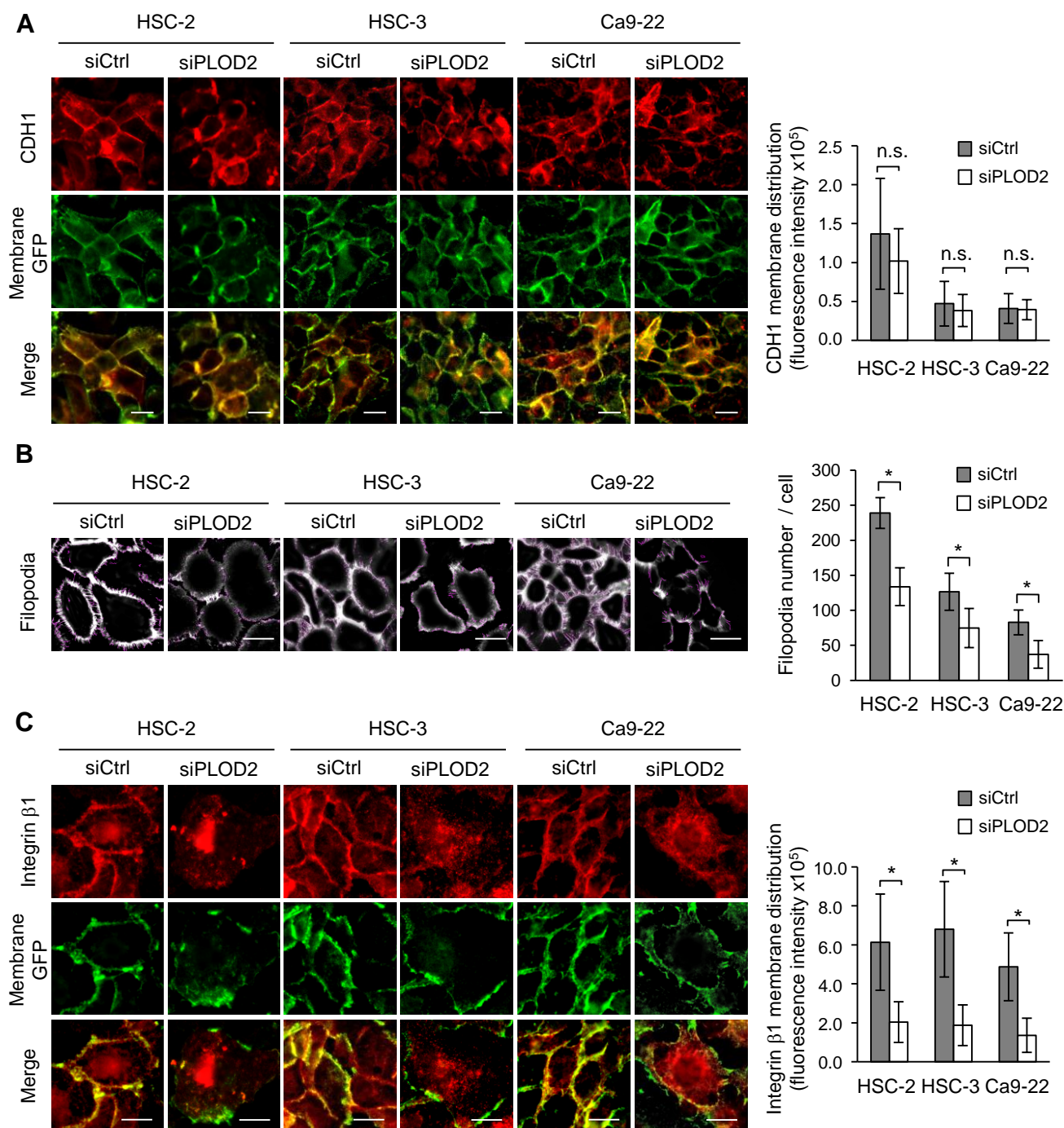
### **PLOD2 Is Essential to Functional Activation of Integrin $\beta$ 1 for Invasion/Metastasis in Head and Neck Squamous Cell Carcinomas**

**Yushi Ueki, Ken Saito, Hidekazu Iioka, Izumi Sakamoto, Yasuhiro Kanda, Masakiyo Sakaguchi, Arata Horii, and Eisaku Kondo**



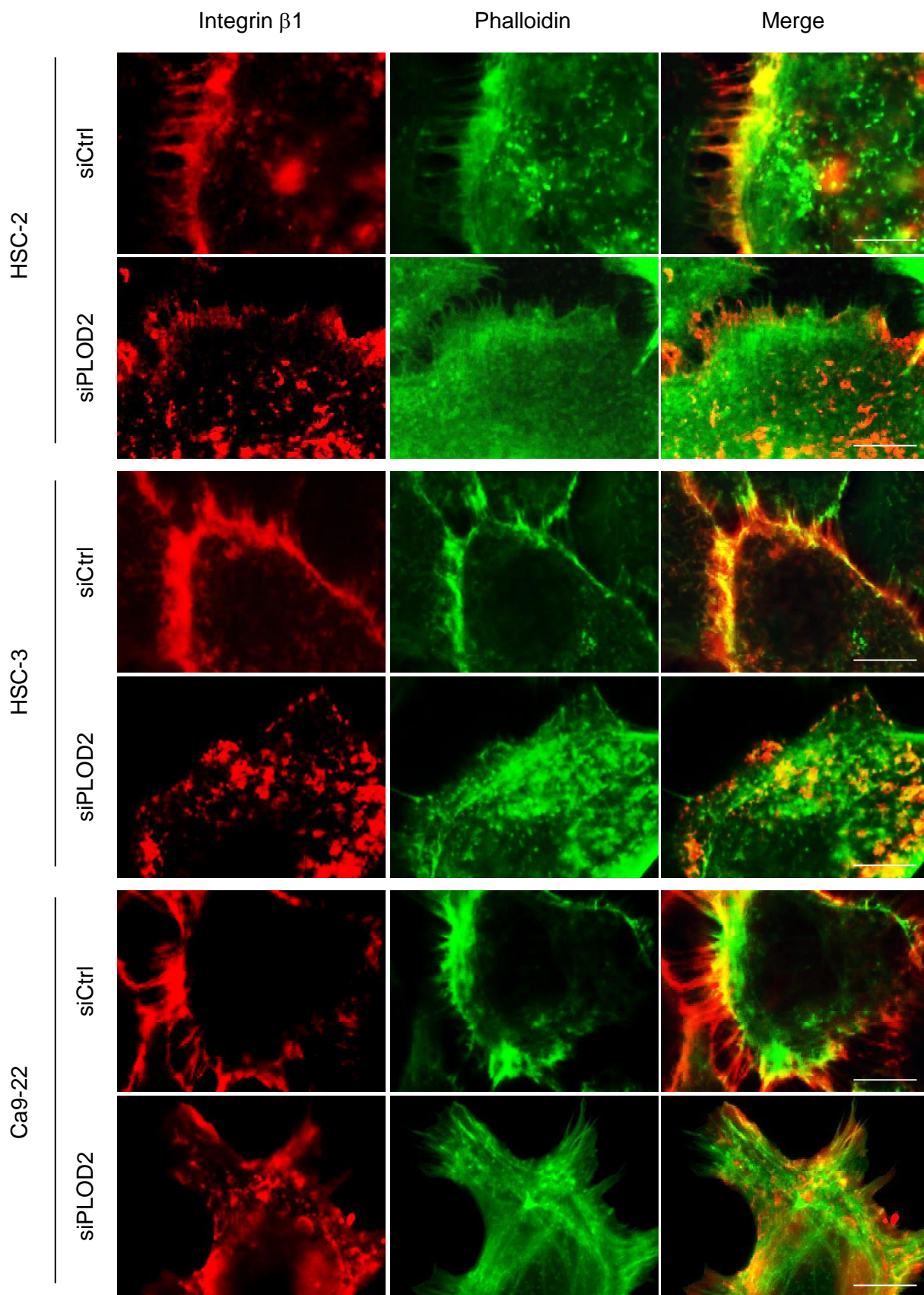
**Figure S1. Cell growth and migration by the suppression of PLODs, Related to Figure 1.**

(A) mRNA expression of the protein hydroxylases was semi-quantitatively examined in oral SCC lines (HSC-2, HSC-3 and Ca9-22) and non-neoplastic keratinocytes (HaCaT) by RT-PCR. (B) Effects of two different oligos for PLOD2 knockdown were confirmed by immunoblot and wound healing assay. #1: custom siRNA synthesis based on previously reports (Sada et al., 2016). #2: on-target plus siRNA (set of 4 oligos). (C) Oral SCC cell growth was measured by MTT assay 48 hours after transfection of siRNA. Data are means  $\pm$  s.d. from 3 biological replicates. (D) Distribution of integrin  $\beta$ 1 (red) by the knockdown of PLOD1 and PLOD3 gene. Cytoskeleton (green) and nuclei (blue) were stained with phalloidin and Hoechst, respectively. Scale bar = 20  $\mu$ m

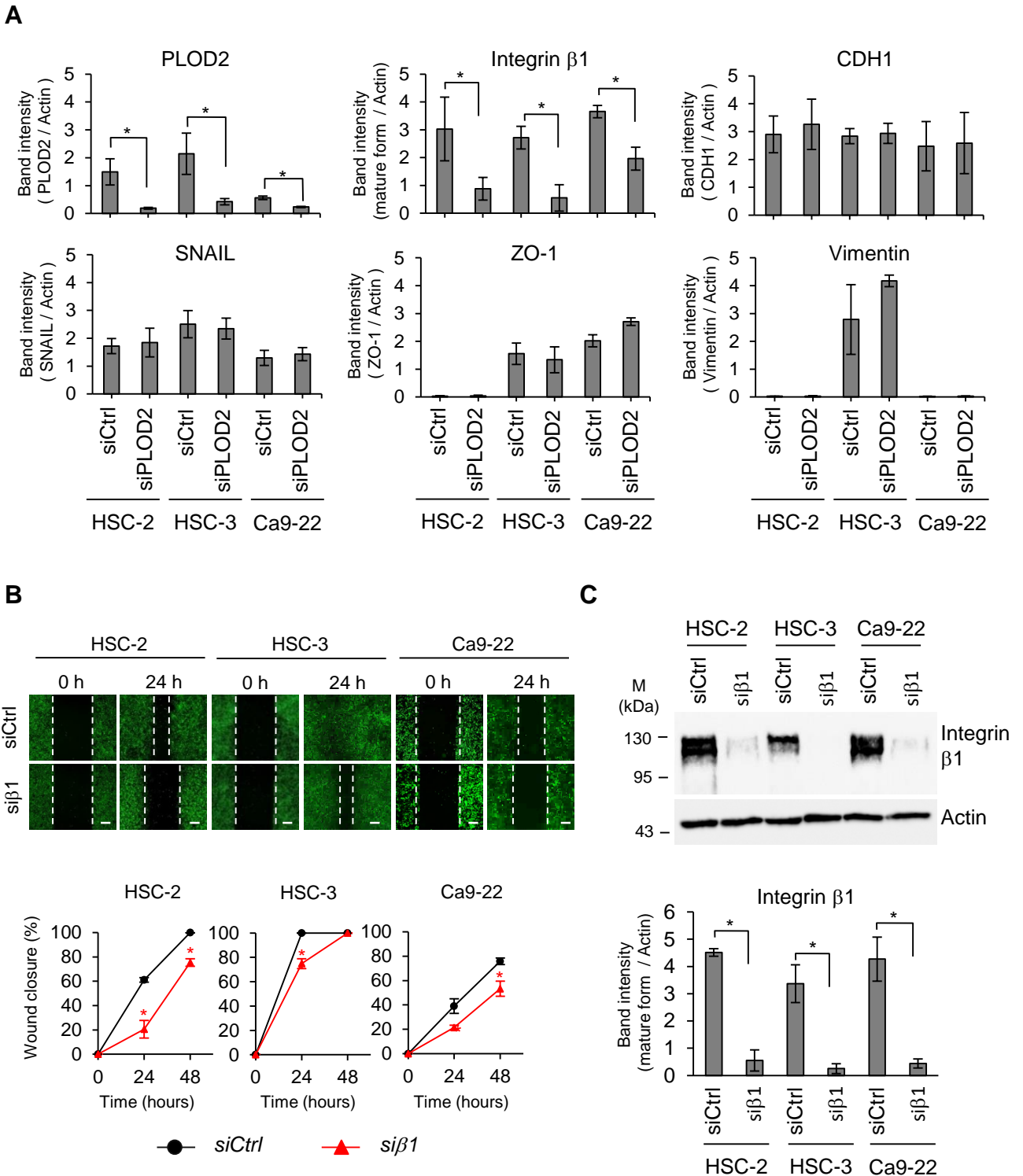


**Figure S2. Membrane localization of CDH1 and integrin  $\beta$ 1 in the PLOD2-knockdown oral cancer cells, Related to Figure 2.**

(A) Representative images of plasma membrane localization of CDH1 (red). Plasma membrane was marked with GFP (green) using a CellLight membrane-GFP. Membrane localization of CDH1 merged with GFP were quantified by fluorescence intensity (right panel). Quantitative results are mean  $\pm$  s.d. from 3 biological replicates with more 10 cells per replicates (n.s. = not significant, Student's t-test). Non-targeting siRNA (siCtrl) and siPLOD2 are shown by gray and white box, respectively. Scale bar = 20  $\mu$ m (B) PLOD2-knockdown cells were stained for integrin  $\beta$ 1, and filopodial protrusions (magenta) were detected by FiloQuant (Jacquemet et al., 2017) as a plugin for the ImageJ. Protrusion number (right panel) was quantified by FiloQuant analysis. Results are mean  $\pm$  s.d. from 3 biological replicates with 20 - 50 cells per replicates (\* $p$  < 0.05, Student's t-test). Scale bar = 20  $\mu$ m (C) Representative images of plasma membrane localization of integrin  $\beta$ 1 (red). Plasma membrane was marked with GFP (green) using a CellLight membrane-GFP. Fluorescence intensity of integrin  $\beta$ 1 localized membrane was calculated and the results are mean  $\pm$  s.d. from 3 biological replicates with more 10 cells per replicates (\* $p$  < 0.05, Student's t-test). Scale bar = 20  $\mu$ m

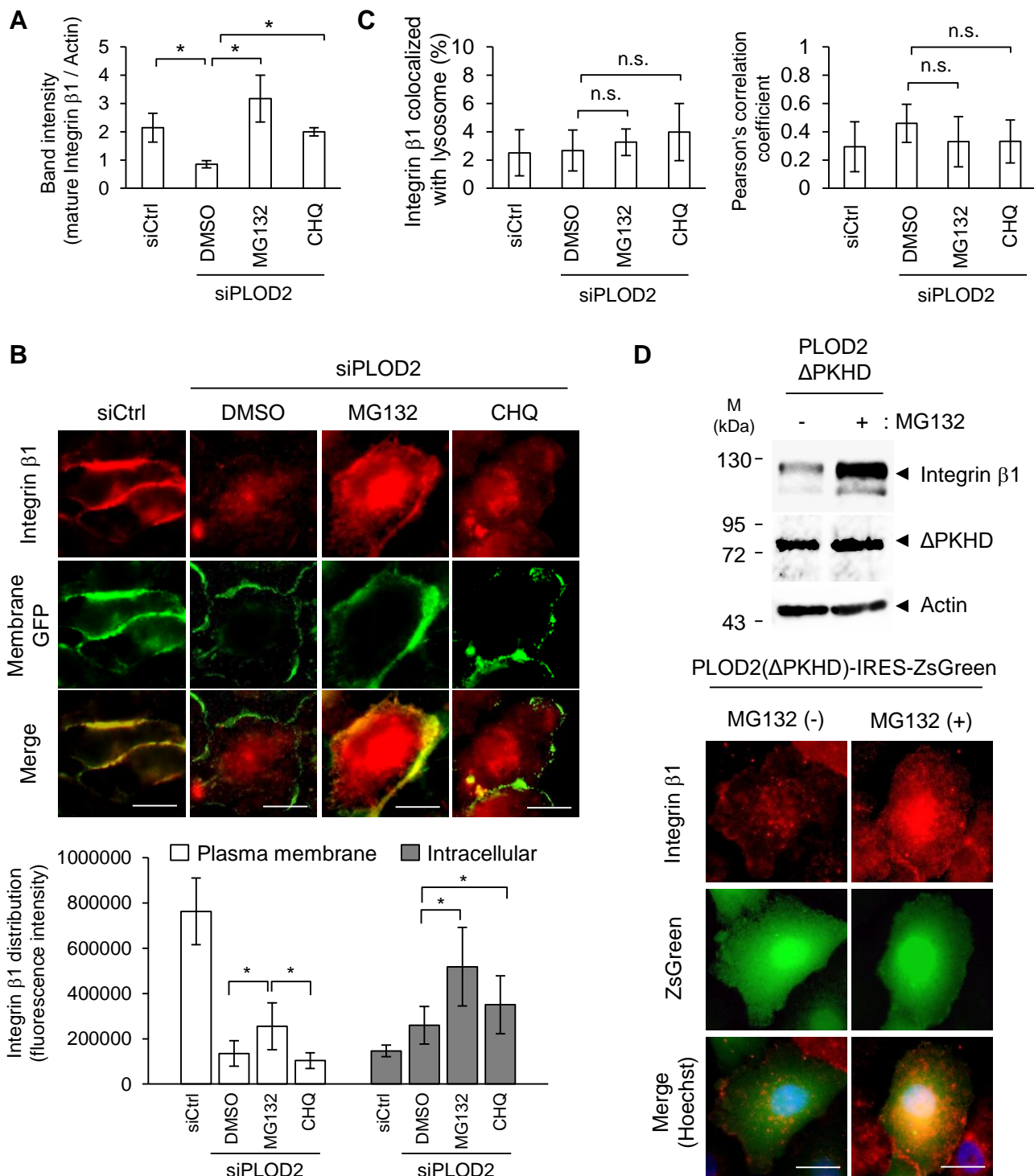


**Figure S3. Intracellular localization of integrin  $\beta$ 1, Related to Figure 2.**  
 Magnification of image in Figure 2B. Scale bar = 10  $\mu$ m.



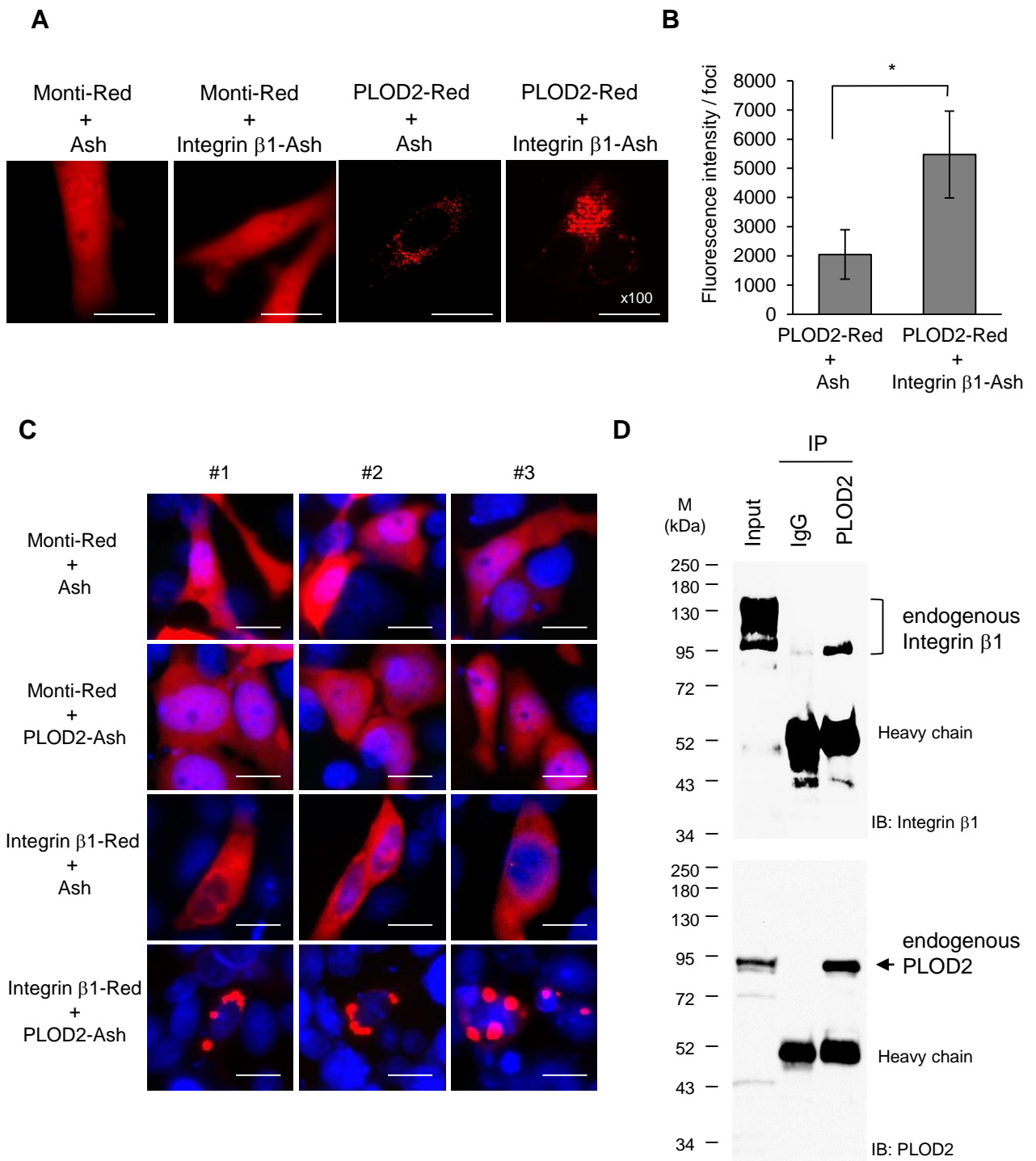
**Figure S4. Expression of integrin  $\beta$ 1 in the PLOD2-knockdown oral cancer cells, Related to Figure 2.**

(A) The intensity of immunoblot band (Fig. 2C) was quantified by densitometric analysis. Band intensity was normalized to beta-Actin band intensity. Data are means  $\pm$  s.d. from 3 biological replicates (\* $p$  < 0.05, Student's  $t$ -test). (B) Cell migration was detected by wound healing assay after transfection of integrin  $\beta$ 1 siRNA (si $\beta$ 1). Images were taken 0 and 24 h after wound formation (scale bar = 400  $\mu$ m), and the wound width was estimated using fluorescence microscopic images. Data are means  $\pm$  s.d. from 3 technical replicates for 1 biological replicate (\* $p$  < 0.05, Student's  $t$ -test as compared to siCtrl). (C) Expression of integrin  $\beta$ 1 in the si $\beta$ 1-transfected cells by immunoblotting using anti-integrin  $\beta$ 1. Band intensity was normalized to beta-Actin band intensity. Data are means  $\pm$  s.d. from 3 technical replicates for 1 biological replicate (\* $p$  < 0.05, Student's  $t$ -test).



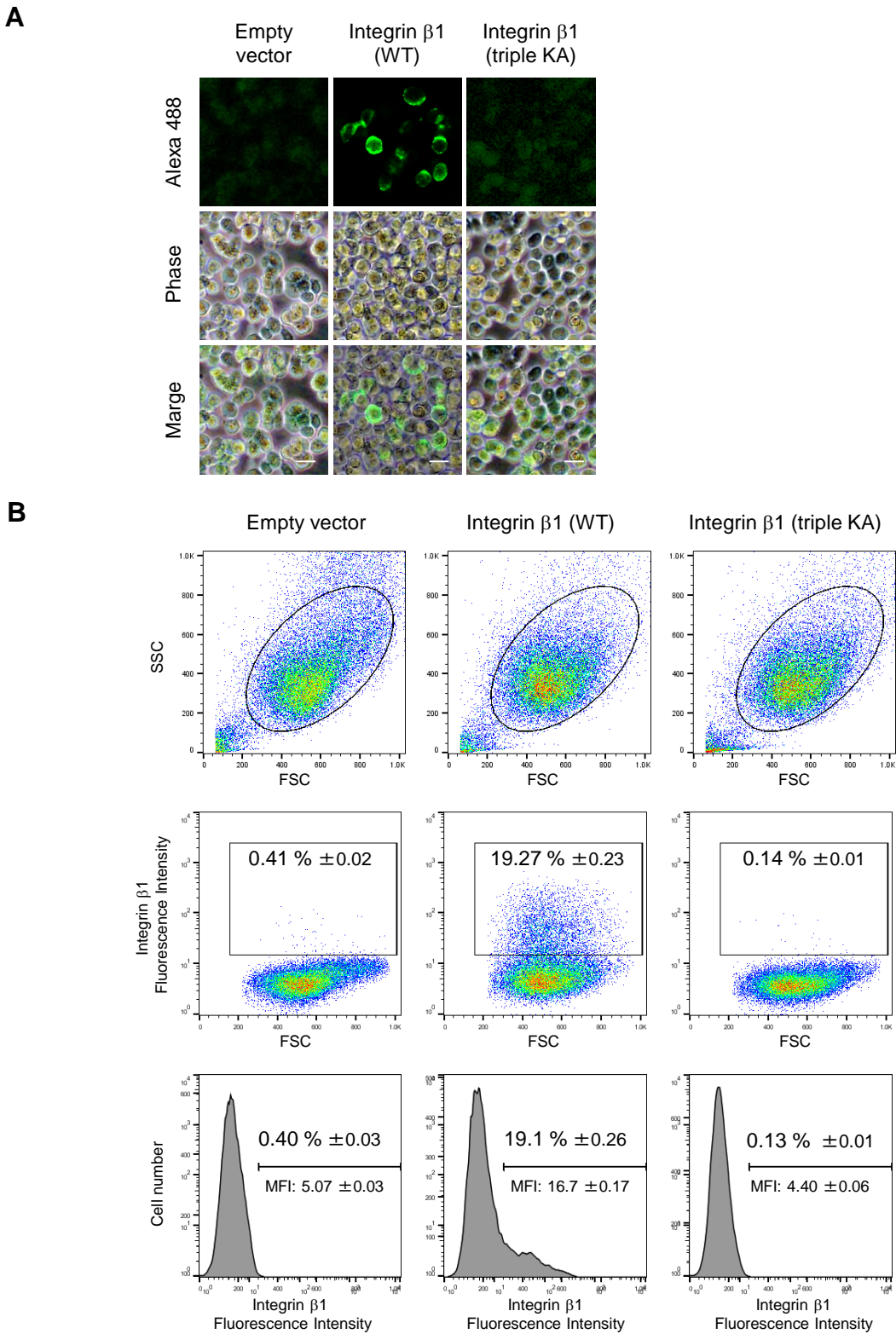
**Figure S5. Distribution of integrin β1 by PLOD2 expression, Related to Figure 2.**

(A) The intensity of immunoblot band (Fig. 2F) was quantified by densitometric analysis. Band intensity was normalized to beta-Actin band intensity. Data are means  $\pm$  s.d. from 3 biological replicates (\* $p < 0.05$ , Student's t-test). (B) Representative images of plasma membrane localization of integrin β1. Distribution shift of integrin β1 were quantified by fluorescence intensity of intracellular and plasma membrane-localized β1. Quantitative results are mean  $\pm$  s.d. from 3 biological replicates with more 10 cells per replicates (\* $p < 0.05$ , Student's t-test). Scale bar = 20  $\mu$ m (C) The percentages of lysosome localization of integrin β1 were calculated by immunofluorescence image of β1 overlap with lyso-GFP vs total β1. Pearson's correlation coefficient was used to measure correlation between integrin β1 and lysosome. Quantitative results are mean  $\pm$  s.d. from 3 biological replicates with more 10 cells per replicates (n.s. = not significant, Student's t-test). (D) HSC-2 cells were transfected with the expression vector of *APKHD-PLOD2* cloning to pEF1a-IRES-ZsGreen. After 24h, the cells were treated with MG132. The expression levels and subcellular localization of integrin β1 were observed by immunoblot and immunocytochemical analysis. Scale bar = 20  $\mu$ m



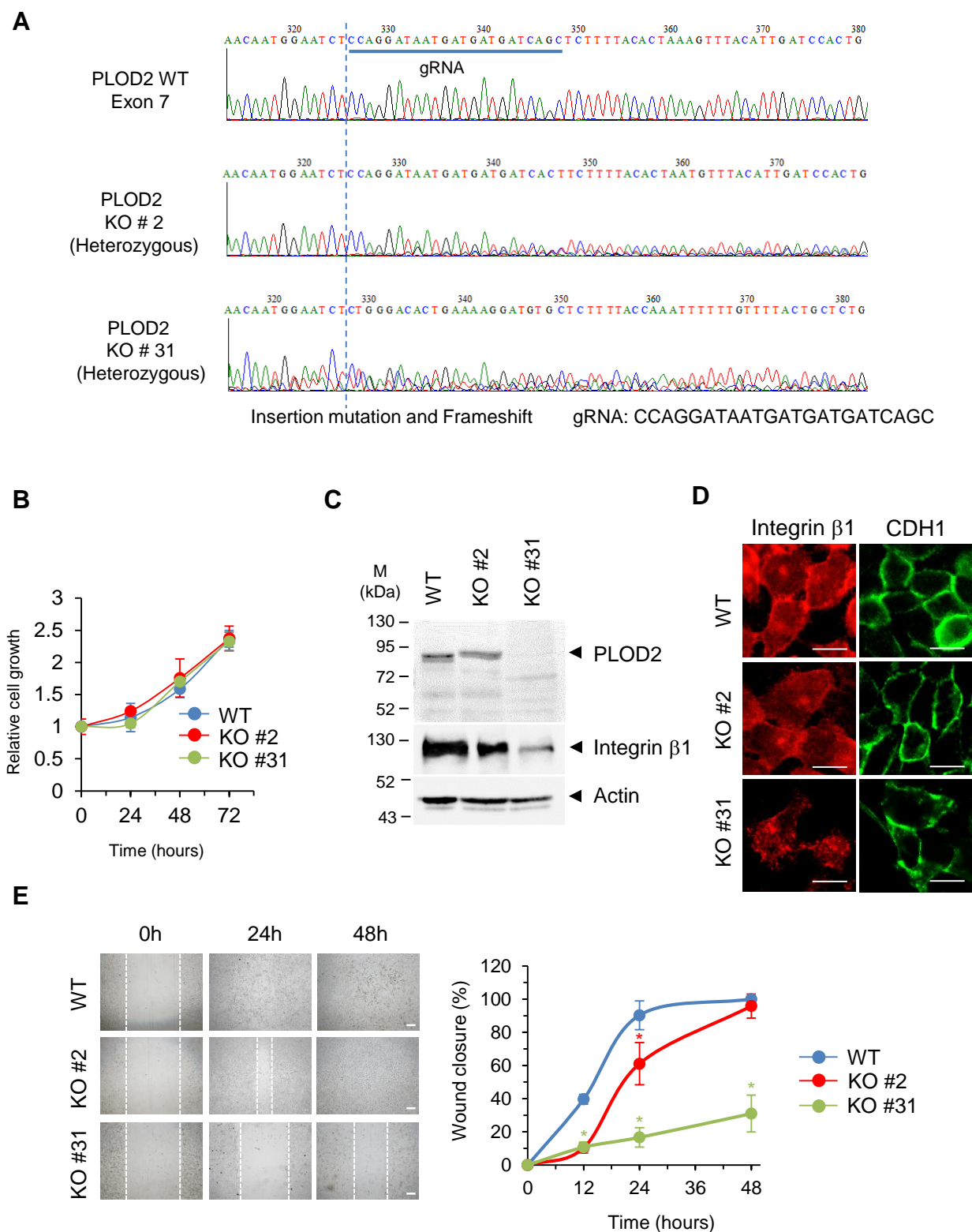
**Figure S6. The interaction of integrin  $\beta$ 1 with PLOD2 in endoplasmic reticulum, Related to Figure 3.**

(A) The protein-protein interaction between PLOD2 and integrin  $\beta$ 1 was detected using the fluorescent-based Fluoppi system. Representative images of intracellular foci were observed at high-resolution by the fluorescence microscopy. Scale bar = 10  $\mu$ m (B) The fluorescence intensity per unit area of foci was measured. Data are obtained as the averages of nine spots from three independent biological replicates. Error bar represent s.d. (\* $p < 0.05$ , Student's t-test). (C) Marked aggregation of fluorescent dots was detected only in the PLOD2-knockout HSC-2 cells cotransfected with integrin  $\beta$ 1-Red and PLOD2-Ash. Nuclei (blue) were stained with Hoechst. Results represent the three images from three independent biological replicates. Scale bar = 20  $\mu$ m (D) Lysate (Input) from HSC-2 cells was immunoprecipitated (IP) with control IgG or anti-PLOD2 antibody. Endogenous integrin  $\beta$ 1 was coprecipitated with endogenous PLOD2 in HSC-2 cells.



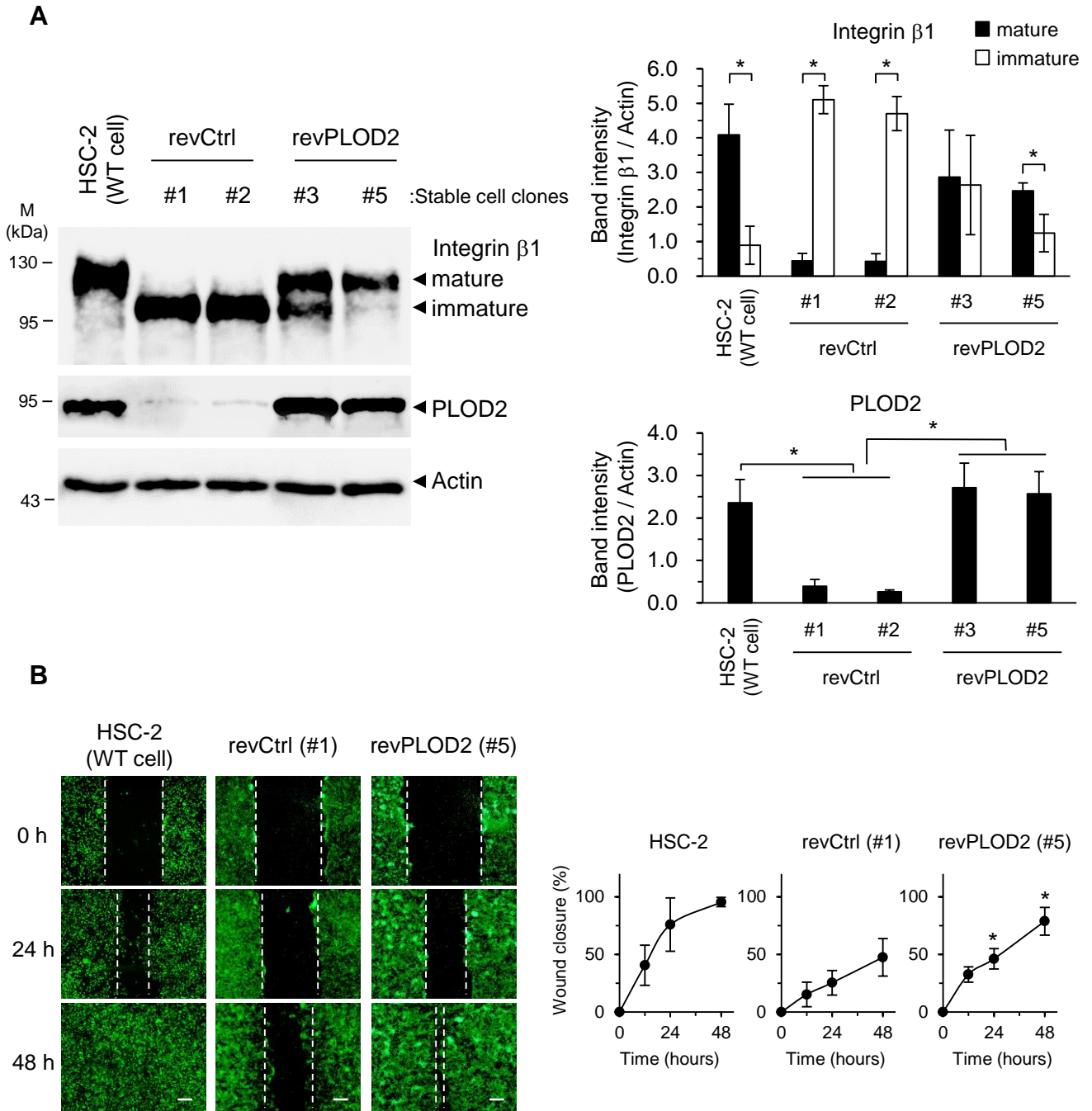
**Figure S7. PLOD2 activity and plasma membrane translocation of integrin  $\beta 1$ , Related to Figure 4.**

(A) BHK (baby hamster kidney) cells were transfected with empty control vector, WT-integrin  $\beta 1$  (WT) and mutant integrin  $\beta 1$  (triple KA). Expression of integrin  $\beta 1$  was confirmed by immunofluorescence staining without permeabilization. Scale bar = 20  $\mu$ m (B) Flow-cytometry analysis of integrin  $\beta 1$  expression in transfected BHK cells without permeabilization. Cells were gated on the basis of their SSC and FSC (upper panels). In dot plot (middle panels), the boxed area shows the positive populations of cell surface. Histogram and mean fluorescence intensity (MFI) shown in lower panels.



**Figure S8. Analysis of PLOD2 KO cells, Related to Figure 5.**

(A) Sequence of Exon 7 in PLOD2 gene targeting by CRISPR-Cas9 system. PLOD2 knockout cells (KO #2, #31) were isolated as heterozygous deletion and frameshift mutation. gRNA (guide RNA) for using CRISPR-Cas9 system are shown. (B) Cell growth of PLOD2-KO HSC-2 cell was measured by MTT assay. Results are mean  $\pm$  s.d. from 3 biological replicates. (C) Expression of PLOD2 and integrin  $\beta$ 1 in the PLOD2-knockout cells were examined by immunoblotting. (D) Distribution of integrin  $\beta$ 1 (red) and E-cadherin (CDH1: green) by the knockout of PLOD2 gene. Scale bar = 20  $\mu$ m (E) Cell migration of PLOD2-knockout cell lines was detected by wound healing assay using 24-well plate coated with collagen. Images were taken 0, 24 and 48 h after wound formation (scale bar = 400  $\mu$ m), and the wound width was estimated using microscopic images. Results are mean  $\pm$  s.d. from 3 technical replicates for 1 biological replicate (\* $p$  < 0.05, Student's t-test as compared to WT).



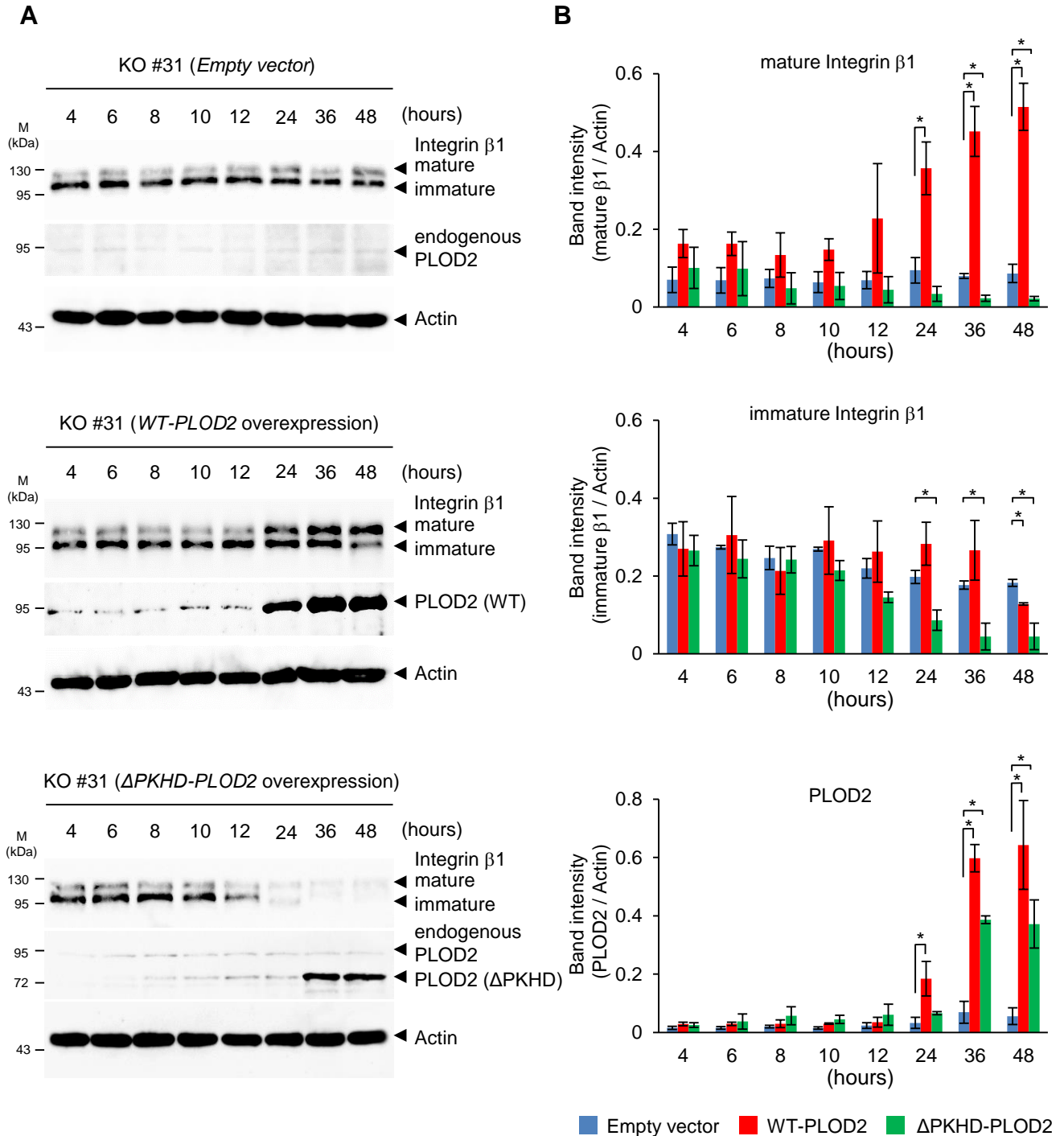


**Figure S10. Integrin  $\beta$ 1 maturation in a PLOD2-dependent manner, Related to Figure 5.**

(A) PLOD2-knockout cells (KO #31) were transiently transfected with empty control vector (upper panel), *WT-PLOD2* (middle panel) and  *$\Delta$ PKHD-PLOD2* (lower panel). Cell lysate was collected at each time points after transfection, and the expression of integrin  $\beta$ 1 and PLOD2 were detected by immunoblotting.

(B) The intensity of immunoblot band was quantified by densitometric analysis. Band intensity was normalized to beta-Actin band intensity. Each band intensity of empty vector, WT-PLOD2 and  $\Delta$ PKHD-PLOD2 overexpression are shown by blue, red and green box, respectively. Data are means  $\pm$  s.d. from 3 biological replicates (\* $p < 0.05$ , Student's t-test as compared to empty vector).

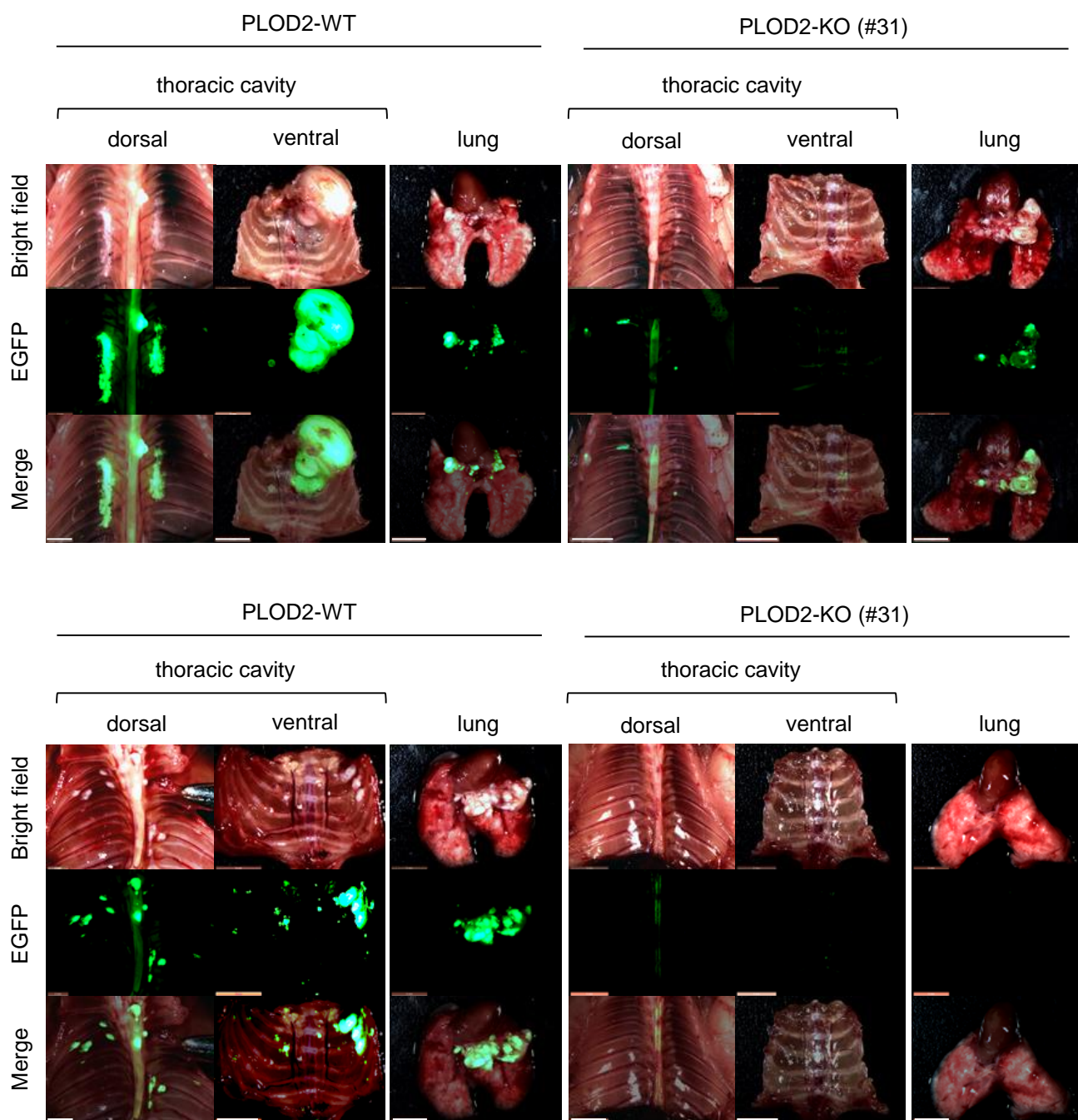


**Figure S11. Fluorescence imaging of PLOD2 KO cells *in vivo*, Related to Figure 5.**

Fluorescence imaging of the invasive and metastatic tumors in the thoracic cavity of mice injecting PLOD2-WT and PLOD2-KO HSC-2 cells are shown. Scale bar = 50  $\mu$ m

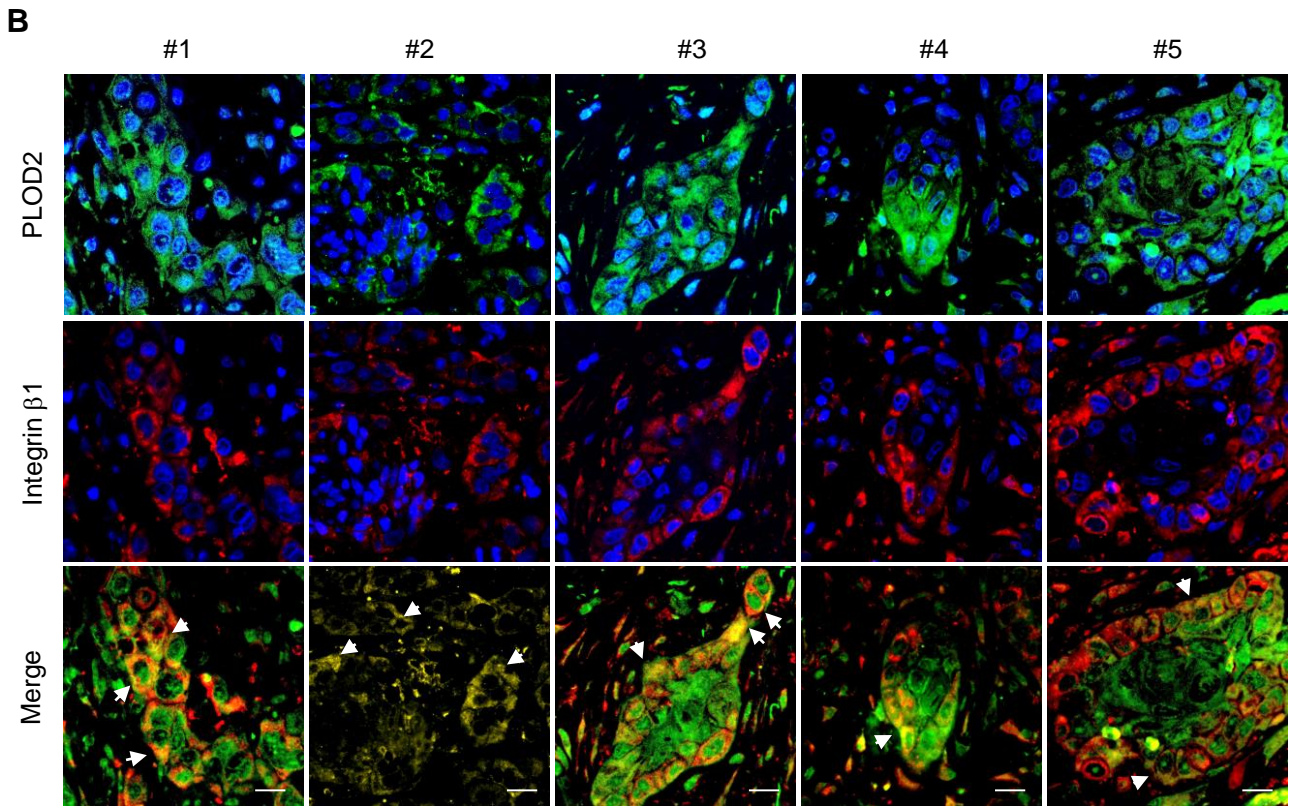
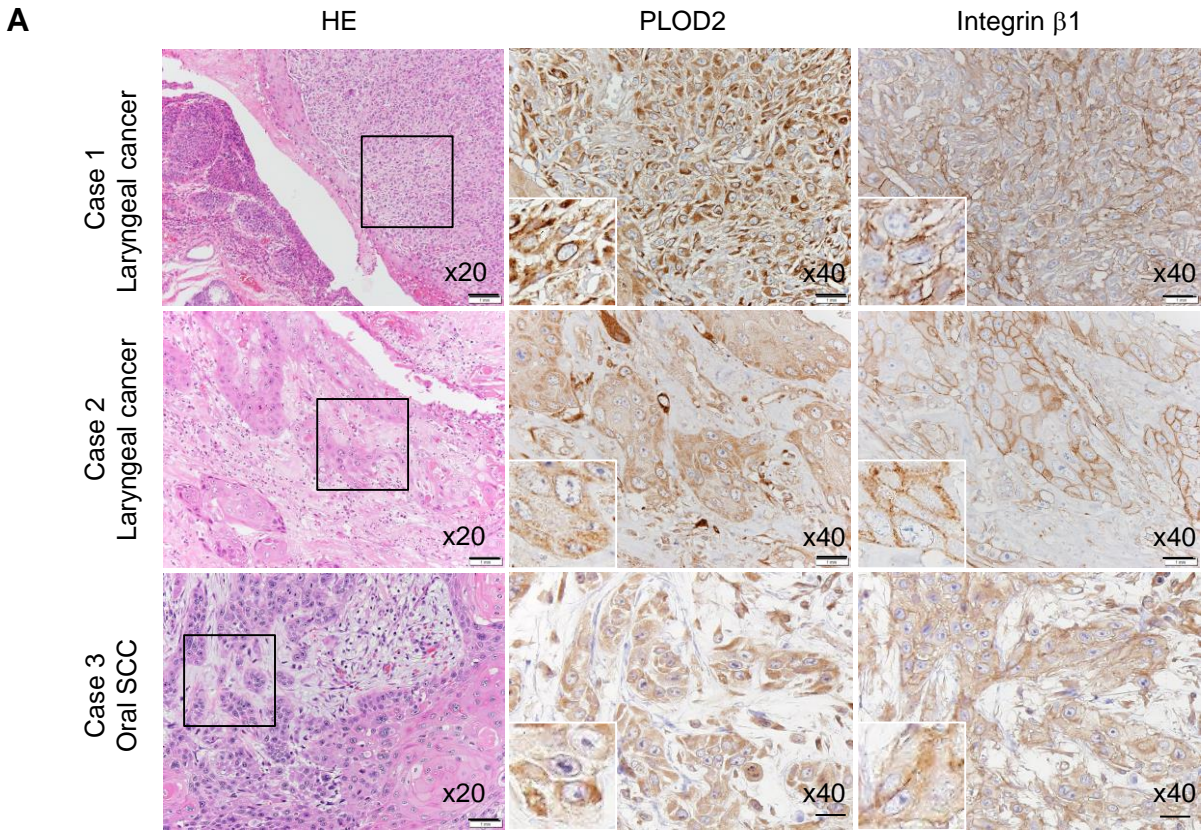
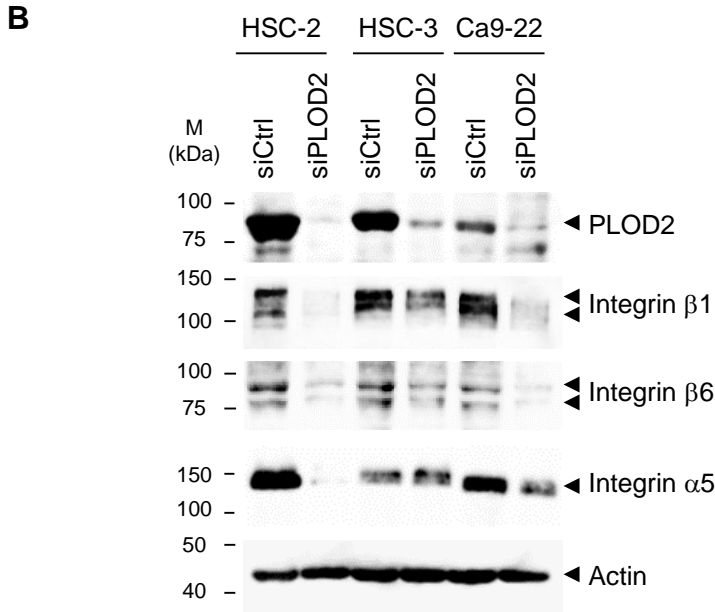
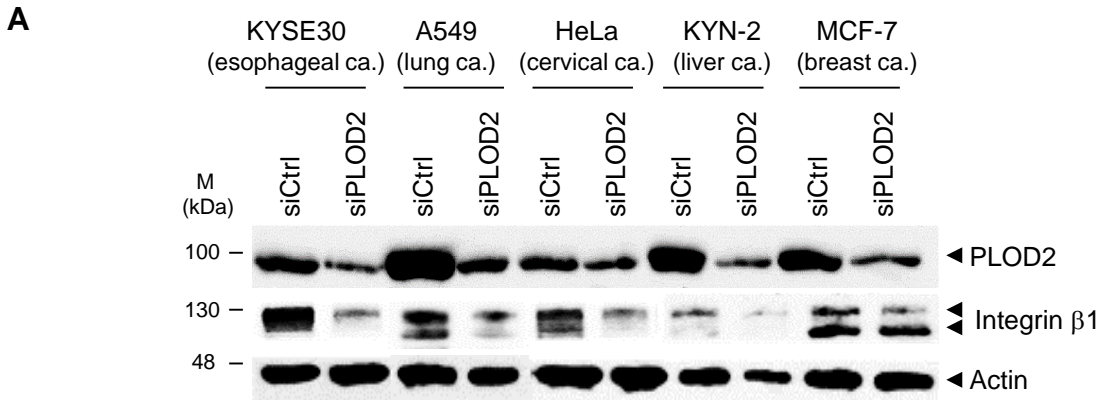


**Figure S12. Colocalization of PLOD2 and integrin  $\beta$ 1 in the SCC tissues, Related to Figure 6**

(A) Immunohistochemistry using anti-PLOD2 Ab and anti-integrin  $\beta$ 1 Ab were performed on the SCC tissues derived from larynx and oral cavity. Box at the HE images (left panel) indicated the field shown as hyperview in the middle and lower panel. Scale bar = 1 mm (B) Subcellular colocalization (lower panels, arrowhead) of PLOD2 (green) and integrin  $\beta$ 1 (red) in each case of oral SCC was assessed by fluorescent immunostaining using anti-PLOD2 and anti-integrin  $\beta$ 1 antibodies. Nuclear counterstain with Hoechst 33258 was applied. Results represent the images from five independent area for the three cases. Scale bar = 20  $\mu$ m



**C**

```

1  MNLQPIFWIG  LISSVCCVFA  QTDENRCLKA  NAKSCGECIQ  AGPNCGWCTN
51  STFLQEGMPT  SARCDLEAL  KKKGCPPDDI  ENPRGSKDIK  KNKNVTNRSK
101  GTAELKLPED  ITQIQPQQLV  LRLRSGEPQT  FTLKFKRAED  YPIDLYYLM
151  LSYMKDDLE  NVKSLGTDLM  NEMRRITSDF  RIGFGSFVEK  TVMPYISTTP
201  AKLRNPCTSE  QNCTSPFSYK  NVLSLTNKGE  VFNELVGKQR  ISGNLDSPEG
251  GFDAIMQVAV  CGSLIGWRNV  TRLLVFSTDA  GFHFAGDGKL  GGIVLPNDGQ
301  CHLENNMYTM  SHYYDYPSIA  HLVQKLSENN  IQTIFAVTEE  FQPVKELKN
351  LIPKSAVGTL  SANSSNVIQL  IIDAYNSLSS  EVILENGKLS  EGVTSYKSY
401  CKNGVNGTGE  NGRKCSNISI  GDEVQFEISI  TSNKCPKDS  DSFKIRPLGF
451  TEEVEVILQY  ICECEQSEG  IPESPKCHEG  NGTFECGACR  CNEGRVGRHC
501  ECSTDEVNSE  DMDAYCRKEN  SSEICSNNGE  CVCQCVCRCR  RDNTNEIYSG
551  KFCECDNFNC  DRNGLICGG  NGVCKCRVCE  CNPNYTGSA  DCSLDTSTCE
601  ASNGQICNGR  GICECGVCKC  TDPKFQGQTC  EMCQTCLGVC  AEHKECVQCR
651  AFNKGEKKDT  CTQECSYFNI  TKVESRDKLP  QPVQPDVSH  CKEKDVDWCW
701  FYFTYSVNGN  NEVMHVVEN  PECPTGPDII...PIVAGYVAGI...VLIIGLALLLI
751  WKLLMIIHDR  REFAKFEKEK  MNAKWDTGEN  PIYKSAVTTV  VNPKYEGK

```

**Figure S13. Expression of integrin β1 in PLOD2-knockdown cancer cells, Related to Figure 4.**

(A) Expression levels of integrin β1 in PLOD2 siRNA-transfected cancer cell lines were detected by immunoblotting. KYSE30 (esophageal cancer), A549 (lung cancer), HeLa (cervical cancer), KYN2 (liver cancer) and MCF7 (breast cancer) were used. (B) Expression of integrin β1, β6 and α5 in the PLOD2-knockdown cells were examined by immunoblotting. (C) Amino acid sequence of integrin β1. Hydroxylation site (box), transmembrane domain (dashed line) and cytoplasmic domain (under line) are shown.

**Table S1. Oligonucleotides, Related to Figures 1 – 4.**

Gene name	Forward primer (5' to 3')	Reverse primer (5' to 3')
<b>Primer sets of quantitative real-time PCR</b>		
ALKBH3	TGGCTTTGTTGACGTGAAAG	GTGCCAGTGAGGATTTGGTT
ASPH	GGGAGATTTTATTTCCACCTGGG	CCTTTGGCTTTATCCATCACTGC
EGLN1	GCCCAGTTTGCTGACATTGAAC	CCCTCACACCTTTCTCACCTGTTAG
EGLN2	AGCCCCAAGTCAGGCTCTC	AGTGGTAGAGGTGGCTGTGG
EGLN3	ATCGACAGGCTGGTCCTCTA	CTTGGCATCCCAATTCTTGT
FIH1	GTGGGCAGGAAGATTGTCAT	GGGTGATGAACAGGGTATGG
FTO	GAGAGCGCGAAGCTAAGAAA	AATGAGGATGCGAGATACCG
ITGB1	AATGAAGGGCGTGTGGTAG	CGTTGCTGGCTTCACAAGTA
JMJD2A	CCTCACTGCGCTGTCTGTATGATC	CCAGTCGAAGTGAAGCACATTC
JMJD6	GGCACAACTACTACGAGAGC	TTTGGCACCTTGTAGTCTTCC
MINA53	TACTTTGGCTCCTTGGTTGG	GGAGTGTCGCTTGATGAAT
NO66	TGTTTACGGGCTTCCAATTC	TCCCCACTCTCACAACTC
OGFOD1	TTTGAAGATTTCCGGTCCTGG	GACCATGAAACCAGCCACTT
PLOD1	GCAGCAGGATGTGTTTCATGT	GGGCTTTGGTGTAGTTCTGG
PLOD2	GCGTTCCTCTCGTCCTCATC	GTGTGAGTCTCCAGGATGC
PLOD3	GGTACGAGGACCAGTGGCT	GAAGGTGGATGAGTCGTGGT
TET1	GGGCAGTGGAAAAGAAACCT	GGGGTTCGGTTTCACTTTTT
beta-Actin	CCTCATGAAGATCCTCACCGA	TGCCAATGGTGATGACCTGG
<b>Primer sets of Cloning and plasmid construction</b>		
PLOD2-WT for pEF1-IRES-ZsGreen	TTACTAGTGCCATGGGGGGATGCACG GTGAAG	ACCCGGGGGATCTATAAATGACACTGC
PLOD2-WT for pcDNA3.1(+)	Same forward primer with PLOD2-WT	TTGCGGCCGCTCAGAGGTCTTCTTCTG AGAT
PLOD2-ΔPKHD for pEF1-IRES-ZsGreen	Same forward primer with PLOD2-WT	ACCCGGGAAATATGGGGAACCAAAAG C
PLOD2-ΔPKHD for pcDNA3.1(+)	Same forward primer with PLOD2-WT	TTGCGGCCGCTCAGAGGTCTTCTTCTG AGAT
PLOD2-Red for pMonti-Red-MNL	GGGAAGCTTACCATGGGGGGATGCAC GGTGAAG	GGCGGCCGCGGATCTATAAATGACAC TGC
Integrin β1-WT for pcDNA3.1(+)	GGGGGATCCACCATGAATTTACAACC AATTTTCTG	TCTCTCGAGCTTTTCCCTCATACTTCG GATTGAC
Integrin β1-Ash for pAsh-MNL Ver.2	Same forward primer with ITGB1-WT	AGCGGCCGCTTTTCCCTCATACTTCGG ATTGA
EGFP for pcDNA3.1(+)	TTTCTCGAGGTGAGCAAGGGCGAGGA GCTGTTC	CGCGGGCCCTTACTTGTACAGCTCGTC CAT
<b>Annealing oligonucleotides</b>		
Myc-tag for PLOD2-WT & ΔPKHD	GGGGGATCCGGCGGAGGGGAGCAGAA GCTCATCTCAGAAGAAGACCTCTGAT	GATCATCAGAGGTCTTCTTCTGAGATG AGCTTCTGCTCCCCCTCCGCCGGATCCC CC
FLAG-tag for Integrin β1-WT & mutants	TCGAGACTACAAAGACGATGACGACA AGTAATAGGCC	TATTACTTGTCTCATCGTCTTTGTAG TC
Myc-tag for EGFP	CTAGCACCATGGAGCAGAAGCTCATC TCAGAAGAAGACC	TCGAGGTCTTCTTCTGAGATGAGCTTC TGCTCCATGGTG

## **TRANSPARENT METHODS**

### **Cell lines**

Human cancer cell lines used in the present study were as follows: HSC-2, HSC-3, derived from the lymph nodes of different patients with metastatic poorly differentiated SCC, and Ca9-22 derived from the patients with gingival SCC (JCRB Cell Bank: Japanese Collection of Research Bioresources Cell Bank) (Yamamoto et al., 1986; Momose et al., 1989; Matsui et al., 1998). Cells were maintained in RPMI 1640 containing 10% FBS with 100 unit/mL penicillin and 100 mg/mL streptomycin (Life Technologies) at 37°C with 5% CO<sub>2</sub>. These cell lines were passaged for less than 6 months and then replaced with those of early passages.

### **PLOD2 KO cell lines**

PLOD2 knockout cell clones were generated by CRISPR/Cas-9 based genome engineering technology. The plasmids hCas9 and gRNA\_Cloning Vector were a gift from George Church (Addgene plasmid # 41815 and #41824) (Mali et al., 2013). gRNA vector including PLOD2 targeting sequence (5'- GCTGATCATCATCATTATCC -3') was prepared by following Church lab protocol (<https://media.addgene.org/41824/>). hCas9 and PLOD2 gRNA vector were co-transfected into cells using Lipofectamine

3000 Transfection Reagent (Thermo Fisher Scientific) by following manufacturer's protocol. Single cell cloning was achieved by serial dilution, and genotype of each clones was analyzed by genomic PCR followed by Sanger DNA sequencing. Following primers were used to amplify genomic sequence including PLOD2 targeting site, forward primer: 5'-TCCCTTAGGAGCCTTGGAACA and reverse primer: 5'-ATCCAGCCAGGTGACATAACCA. Sanger DNA sequencing was carried out using the forward primer and BigDye terminator v3.1 cycle sequencing kit (Applied Biosystems).

For revertant cell lines re-expressing PLOD2 in PLOD2-knockout cells, the PLOD2-IRES-ZsGreen plasmid was transfected into PLOD2-knockout cells. After selection with 0.1 mg/ml of Geneticin (G418, Gibco) for 4 weeks, PLOD2 re-expressing stable lines were newly cloned.

### **Animal models**

A total of  $1.0 \times 10^6$  cells of human oral squamous cell carcinoma cell lines stably expressing Green fluorescent protein (GFP-HSC-2) were transplanted into the pleural cavity of a 7-week-old female nude mice (BALB/c nu/nu, CLEA Japan Inc.) by direct injection. 40 days after initial administration of the GFP-HSC-2 cells, all mice were

autopsied and their organs examined by fluorescence stereomicroscopy (Leica M165 FC).

The animal studies in the present work were approved by the Animal Research Committee of the Niigata University School of Medicine. All mouse procedures and euthanasia, including cell transplantations, were performed painlessly or under anesthesia, and within the strict guidelines of the Experimental Animal Center of Niigata University School of Medicine.

### **Plasmid construction and transfection**

cDNA were prepared from HSC-2 cells using an RNeasy kit (Qiagen) and a Super Script III kit (Invitrogen). Human *PLOD2* CDS (NM\_000935.2) and *Integrin  $\beta$ 1* CDS (NM\_002211.4) were amplified from HSC-2 cDNA and NHDF cDNA, respectively. They were cloned into pBluescript SK<sup>+</sup> vector (Stratagene). To generate the *PLOD2* wild type and mutant plasmid, *PLOD2* genes were subcloned into a pEF1-IRES-ZsGreen vector at the *Nhe* I / *Spe* I compatible cohesive sites and *Sma* I site. The synthetic myc-tag oligonucleotides were annealed and inserted into a pEF1-IRES-ZsGreen (Clontech) vector at the *Sma* I and *Bam*H I site. Furthermore, *PLOD2-myc* gene were subcloned into a pcDNA3.1(+) at the *Nhe* I / *Spe* I compatible

cohesive sites and *Not* I site. For integrin  $\beta$ 1-FLAG plasmid, *integrin  $\beta$ 1* gene were subcloned into a pcDNA 3.1(+) vector (Thermo Fisher Scientific) at the *Bam*H I - *Xho* I. The synthetic flag-tag oligonucleotides were annealed and inserted into a pcDNA 3.1(+) vector at the *Xho* I and *Apa* I site. For Myc-EGFP plasmid, *EGFP* gene were amplified from the pEGFP-N1 vector (Clontech) and subcloned into a pcDNA 3.1(+) at the *Xho* I - *Apa* I site. The synthetic myc-tag oligonucleotides were annealed and inserted into the *Nhe* I-*Xho* I sites.

PLOD2-Red plasmid was constructed by cloning the cDNA encoding *PLOD2* into the *Hind* III - *Not* I of the vector pMonti-Red-MNL (MBL). Integrin  $\beta$ 1-Ash plasmid was constructed by cloning the cDNA encoding *integrin  $\beta$ 1* into the *Bam*H I - *Not* I of the vector pAsh-NML Ver.2 (MBL).

The site-directed mutagenesis for integrin  $\beta$ 1 was performed by PCR using a single mutant primer and PfuUltra High-Fidelity DNA polymerase (Agilent Technologies). After *Dpn* I digestion the PCR products were transformed into the competent *E.coli* cells. The nucleotide sequences of all constructs obtained by PCR were confirmed by DNA sequencing. The primer sets used in this study are shown in Table S1.

For the plasmid transfection, Cells were transiently transfected with *PLOD2* and *integrin  $\beta$ 1* plasmids using Lipofectamine 3000 (Thermo Fisher Scientific) according to

the manufacturer's instructions. The stable clone expressing EGFP was selected in 0.6 mg/ml of Geneticin (Gibco).

### **Cell proliferation assay**

Cells ( $4 \times 10^4$ ) were seeded on a 48-well plate. After 48 hours of siRNA transfection, cell proliferation was evaluated by MTT assay using Cell Count Reagent SF (Nacalai Tesque) according to the manufacturer's protocol.

### **Wound healing assay**

The myc-EGFP plasmid was transfected into HSC-2, HSC-3 and Ca9-22 cells. After selection with 600  $\mu$ g/ml of Geneticin for 4 weeks, GFP-expressing stable lines were newly cloned and used in wound healing assay. Cells were seeded in collagen type-1 coated 24-well plates. 48 hours after siRNA treatment was made a scratch using a cell scratcher was done (Iwaki, Asahi Technoglass). The wounded monolayer was washed with PBS, exchanged medium, and photographed using a microscope every time. All data were obtained from at least three independent experiments.

### **Conventional and quantitative PCR**

Total RNA was extracted from prepared cells using RNeasy plus mini kit (QIAGEN) according to the manufacturer's protocol. Complementary DNA was synthesized from 1  $\mu$ g of total RNA using Revertra Ace (Toyobo) for performing mRNA analysis. Each cDNA was amplified by PCR with z-Taq polymerase (TaKaRa). Quantitative real-time PCR was performed using SYBR Green RT-PCR Kit (Applied Biosystems). Data analysis was followed by  $\Delta\Delta$ CT methods using the step one plus instruction (Applied Biosystems). The primer sets used in this study are described in Supplementary Table S1.

### **RNA interference**

Each siRNA (25 nM) was transfected using Lipofectamine RNAi MAX reagent (Thermo Fisher Scientific) according to the manufacturer's protocol. ON-TARGET plus SMART pool siRNA for human PLOD2 (#5352), PLOD1 (#5351) and PLOD3 (#8985) were purchased from Dharmacon. The custom siRNA of PLOD2 (Sada et al., 2016) and integrin  $\beta$ 1 (Kato et al., 2014) was synthesized by Sigma-Aldrich. Negative control scrambled siRNA was purchased from Sigma-Aldrich.

### **Immunoblotting and immunoprecipitation**

The cell pellets were lysed with the RIPA buffer (50 mM Tris/HCl pH 7.5, 150 mM NaCl, 0.5% sodium deoxycholate, 1% NP-40, 0.1% SDS) containing the complete mini protease inhibitor (Roche). Samples were separated on 10% SDS-PAGE gels followed by transfer to PVDF membrane. Nonspecific binding was blocked by incubation in 5% skim milk in TBS-T. Blots were probed with specific primary antibodies followed by appropriate horseradish peroxidase-conjugated secondary antibody. Positive signals were detected by a chemiluminescence system (Supersignal West Pico or Femto substrate; Thermo Fisher Scientific) and quantification of band intensity was calculated using a ChemiDoc Touch imager (Bio-Rad). Anti-PLOD1 (Sigma-Aldrich), anti-PLOD2 (Proteintech), anti-PLOD3 (Sigma-Aldrich), anti-Integrin  $\beta$ 1 (CST) anti-E-cadherin (BD Biosciences), anti-SNAIL (Abcam), anti-ZO-1 (Abcam) anti-Vimentin (Santa Cruz Biotechnology) and anti-Actin (Merck) antibodies were used for immunoblotting.

For immunoprecipitation, HEK 293T cells were transiently co-transfected with the expressor plasmid of integrin  $\beta$ 1-flag and PLOD2-myc. Cells were lysed in IP buffer (50 mM Tris-HCl pH7.5, 150 mM NaCl, 1% Brij 20, 0.5% n-octyl- $\beta$ -D-glucoside, 0.5% Triton-X, 1 mM PMSF) supplemented with protease inhibitors cocktail (Roche). Cell lysates were incubated overnight at 4°C with anti-FLAG M2 affinity gel

(Sigma-Aldrich). Beads were washed six times with wash buffer (50 mM Tris-HCl pH7.5, 150mM NaCl, 0.2% NP-40) and were boiled in 2× sample buffer (125 mM Tris-HCl pH 6.8, 4% SDS, 20% Glycerol, 0.01% Bromophenol blue, 10% β-Mercaptoethanol). Equal amounts of proteins were separated on 10% SDS-PAGE gels and immunoblotted with the anti-myc monoclonal antibody (9E10, Sigma-Aldrich) and horseradish peroxidase-conjugated secondary antibody (Mouse TrueBlot ULTRA: anti-mouse Ig HRP, Rockland).

### **Fluoppi assay**

The protein-protein interaction between PLOD2 and integrin β1 was detected using the fluorescent-based technology detecting protein-protein interaction (Fluoppi) system (MBL life science), in which PPIs were visualized as foci (Koyano et al., 2014; Yamano et al., 2015). PLOD2 was subcloned into a pMonti-Red-MNL plasmid to fuse with a Monti-Red (homo tetramer red fluorescent protein from *Montipora* sp.) tag. Integrin β1 was subcloned into a pAsh-MNL ver.2 plasmid to fuse with an Ash (homo oligomerized protein assembly helper) tag. These plasmids of PLOD2-Red and integrin β1-Ash were co-transfected into HSC-2 or HeLa cells using Lipofectamine 3000 (Thermo Fisher Scientific) according to the manufacturer's instructions, and intracellular foci were

observed by the Olympus IX71 fluorescence microscope and analyzed using cellSens standard software (Olympus).

### **Mass spectrometric analysis of integrin $\beta$ 1**

Extracts of  $5 \times 10^6$  cells expressing the integrin  $\beta$ 1-flag and PLOD2-myc were prepared on ice for 30 minutes in IP buffer. Integrin  $\beta$ 1-flag proteins were immunoprecipitated by using anti-FLAG M2 affinity gel and eluted by  $3 \times$  FLAG peptide. Immunoprecipitated integrin  $\beta$ 1-Flag were separated SDS-PAGE, the gel was then stained with Coomassie Blue, and protein bands corresponding to the proteins of interest were excised and digested with LysC protease (Roche) according to standard protocol. The extracted peptides were desalted and concentrated using RP-C18 StageTip columns and the eluted peptides used for mass spectrometric analysis. All LC/MS-MS experiments were performed by using standard protocol (ACROSCALE Inc. Sendai, Japan). Peptides were analyzed using an amaZon ETD ion trap mass spectrometer (Bruker Daltonics). Spectral data were compared to the Swiss-Prot Homo sapiens database using Mascot (version 2.3.01; Matrix Science) to identify the protein. The search criteria were: trypsin enzyme, allowance of up to two missed cleavage peptides, mass tolerance  $\pm 0.5$  Da, MS/MS tolerance  $\pm 0.5$  Da, fixed modifications of cysteine

carbamido-methylation, variable modifications of lysine hydroxylation.

### **Flow-cytometry**

Human integrin  $\beta 1$  WT and triple KA mutant plasmid was transfected into BHK (baby hamster kidney) cells. Cells were harvested by trypsinization and washed twice with PBS containing 2% FBS. The cells incubated with anti-integrin  $\beta 1$  antibody (Abcam) for 20 min at 4°C, and then washed twice with PBS containing 2% FBS. For detection of  $\beta 1$  integrin, cells were incubated with anti mouse-Alexa fluor 488 (Thermo Fisher Scientific) for 20 min at 4°C, and further washed twice PBS containing 2% FBS. Cells were detected on a BD FACS Calibur cell analyzer (BD Biosciences) and data were analyzed using FlowJo VX software.

### **Purification and activity of PLOD2**

*PLOD2* cDNA were subcloned into the pCMVViR-TSC vector (Sakaguchi et al., 2014) and the PLOD2-myc-6×His expressor was transfected into HEK293T cells. Extracts of  $3 \times 10^6$  cells expressing the PLOD2-myc-6×His were prepared on ice for 30 minutes in IP buffer. Cell lysate was load into a column of TALON metal resin (Takara) and washed twice with wash buffer (50 mM Tris-HCl pH7.5, 150 mM NaCl, 10 mM

imidazole), and further eluted with 150 mM imidazole. The eluted PLOD2 was dialysed with 50 mM HEPES pH7.4 and 150 mM NaCl, and then concentrated with the Amicon ultra-0.5 centrifugal filters (Millipore). Protein concentration was estimated with the BCA protein assay (Pierce), Nanodorp Spectrophotometer at 280 nm (Thermo Fisher Scientific) and CBB staining of SDS-PAGE.

Hydroxylation reaction of PLOD2 were carried out in 50  $\mu$ L volume of reaction buffer based on previously reported method (Guo et al., 2017). Briefly, the purified PLOD2 (approximately 1.0  $\mu$ g) was reacted with the reaction buffer (50 mM HEPES pH7.4, 50  $\mu$ M FeSO<sub>4</sub>, 100  $\mu$ M  $\alpha$ -KG, 500  $\mu$ M ascorbate, 0.125 mM peptide substrate) for 120 min at 37 °C. The collagen peptide substrate (IKGIKGIKG) and integrin  $\beta$ 1 peptide substrate (AFNKGEKK) were synthesized at 95% purity by Scrum Inc (Tokyo Japan). 1  $\mu$ l of the reaction solution was diluted in 25  $\mu$ L of 50 mM HEPES pH7.4 buffer and measured succinate production in the reaction solution using Succinate-Glo assay following the manufacturer's procedure (Promega). The luminescence was detected using a Centro LB 960 microplate luminometer (Berthold).

### **Immunofluorescence**

Cultured cells were fixed with PBS containing 4% paraformaldehyde and washed

with 0.1% Triton X-100 in phosphate-buffered saline (-). PLOD2 was stained with rabbit anti-PLOD2 antibody (Proteintech), Integrin  $\beta$ 1 was stained with mouse anti-integrin  $\beta$ 1 antibody (Abcam) and E-cadherin was stained with mouse anti-E-cadherin antibody (BD Biosciences) as a primary antibody, and further treated with Cy3-labeled goat anti-rabbit (H+L) antibody (Jackson), as a secondary antibody. Cell nuclei were counterstained with 4',6-diamidino-2-phenylindole (Hoechst 33258 dye; Molecular probes). CellLight ER-GFP BacMam 2.0 (Thermo Fisher Scientific) was used for ER marker. For the staining of actin filaments (F-actin), Alexa 488-conjugated phalloidin (Molecular Probes) was used. The fluorescent signals were detected by the Olympus IX71 fluorescence microscope and analyzed using cellSens standard software (Olympus). For quantification, the fluorescence intensity of plasma membrane-localized integrin  $\beta$ 1 vs total integrin  $\beta$ 1 was calculated using Metamorph software (Molecular devices). Colocalization analysis and calculation of filopodial protrusions were performed using a Coloc 2 and FiloQuant (Jacquement et al., 2017) as a plugin for the ImageJ software. CellLight Membrane-GFP BacMam 2.0 (Thermo Fisher Scientific) was used for plasma membrane marker.

### **Immunohistochemistry and patient-derived tissues**

Human oral, pharyngeal and laryngeal carcinoma tissues were fixed in 10% buffered formalin solution. Paraffin-embedded sections were deparaffinized, and antigen retrieval was performed by autoclaving (Pascal S2800, DakoCytomation) in sodium citrate buffer. Then endogenous peroxidase activity was quenched by incubation in 0.3% hydrogen peroxide (Kanto Chemical Co.) for 20 minutes at room temperature. Slides were incubated with a 1:250 dilution of anti-PLOD2 antibody (Proteintech) and anti-integrin  $\beta$ 1 antibody (CST) in CanGet signal immunostain solution B (Toyobo) overnight at 4°C, and further incubated with anti-rabbit HRP antibody (CST). After the slides were washed with phosphate buffered saline (-), they were subjected to the DAB detection system (Nichirei).

The study using patient-derived tissues was approved by the ethics committees of Niigata University and Niigata Cancer Center Hospital. Informed consent for use of materials was also obtained from each patient.

### **Quantification and Statistical Analysis**

Data were represented as mean  $\pm$  standard deviation (s.d.). Comparisons between two groups were carried out using Student's t test (MS Excel). A value of  $P < 0.05$  was considered significant.